FULL PAPER

Syntheses, Crystal Structures, Spectroscopic Properties, and Catalytic Aerobic Oxidations of Novel Trinuclear Non-Heme Iron Complexes

Volker Rabe,[a] Wolfgang Frey,[a] Angelika Baro,[a] Sabine Laschat,*[a] Matthias Bauer,[b]
Helmut Bertagnolli,[b] Subramanian Rajagopalan,[b] Tanja Asthalter,[b] Emil Roduner,[b]
Herbert Dilger,[b] Thorsten Glaser,[c] and David Schnieders[c]

Dedicated to Professor Martin Jansen on the occasion of his 65th birthday

A series of 2,6-diacylpyridine ligand precursors **5a–d**·HCl with different tether lengths between the carboxyl and pyridine moiety was prepared and converted into the correspondig trinuclear $Fe_3(\mu_3\text{-}O)$ complexes **8a–d** and **10**. Under slow precipitation conditions a tetranuclear complex **9** was isolated instead of **8a**. Single-crystal X-ray diffraction analyses were performed on ligands **5a–d** and complexes **9** and **10**. Characterization by X-ray absorption spectroscopy (XAS) proved a trinuclear $Fe_3(\mu_3\text{-}O)$ core for complexes **8a–d**. When complex **8a** was submitted to Gif-type oxidations (O_2, Zn, pyridine, HOAc), Mössbauer and nuclear inelastic scattering (NIS) suggested the formation of mononuclear species. The trinuclear ferric complex **10** has an isosceles molecular structure, which is manifested in the ^{57}Fe Mössbauer spectrum by two quadrupole doublets with a 2:1 intensity ratio. The magnetic measurements reveal two moderate antiferromagnetic exchange interactions of –22.1 and –33.8 cm^{-1}. Spin concentrations of complex **10** were determined by EPR spectroscopy, which supports the Mössbauer and magnetic studies. Complexes **8–10** were employed in catalytic aerobic oxidations of adamantane **11**, cyclohexene **19**, and α-pinene **23**. For adamantane **11**, the oxidation of secondary C–H bonds to the corresponding ketone **14** is favored. In addition, adamantylpyridines **15–18** were isolated, thus supporting a radical pathway. A strong preference of allylic oxidation versus epoxidation was found for cyclohexene **19** and α-pinene **23**. (© Wiley-VCH Verlag GmbH & Co. KGaA, 69451 Weinheim, Germany, 2009)

Introduction

The understanding of the operating mode of non-heme enzymes such as methane monooxygenase and ribonucleotide reductase is currently a major challenge because of the biomimetic oxidations of hydrocarbons employing dioxygen. Theoretical and experimental studies on synthetic model complexes by various research groups have provided insight into catalytic cycles, reactive intermediates, competing energy profiles, and product distributions.[1] However, these model complexes are often limited by low selectivities and turnover numbers, poor stability, stoichiometric amounts of oxidants, or difficulty in varying the ligand system. Thus, there is still a need for novel non-heme iron complexes, whose ligand systems can be varied easily in order

to improve the catalytic properties. Since the seminal work by Barton[2] on Gif-type oxidations of hydrocarbons employing an iron catalyst in the presence of a reducing agent under 1 atm O_2 in pyridine/acetic acid and his finding that the trinuclear μ-oxo iron complex $Fe_3(\mu_3\text{-}O)(OAc)_6L_3$ (L = py, H_2O)[3] is particularly suited for this purpose,[2a,2b] Barton and several groups focused on bi-, tri- and tetranuclear μ-oxo iron complexes and investigated their structural, spectroscopic, and mechanistic aspects.[4–6]

As reported by Barton, mononuclear iron picolinate or iron 1,10-phenthroline-2-carboxylate complexes have been used as oxidation catalysts.[5y] However, iron complexes bearing pyridine carboxylate or pyridine dicarboxylate ligands are prone to ligand degradation under oxidative conditions.[7] In order to circumvent this problem, we prepared pyridine dicarboxylate ligand precursors **5a–d**, in which the carboxyl group is separated from the pyridine moiety by an alkyl spacer. By adjusting the spacer lengths, it should be possible to obtain iron complexes with different nuclearity, stability and catalytic properties. In particular, we have focused on the detailed spectroscopic investigation of the iron complexes. These data should allow further optimization of the catalytic properties even if one considers that these pre-

[a] Institut für Organische Chemie, Universität Stuttgart,
    Pfaffenwaldring 55, 70569 Stuttgart, Germany
    Fax: +49-711-685-64285
    E-mail: sabine.laschat@oc.uni-stuttgart.de
[b] Institut für Physikalische Chemie, Universität Stuttgart,
    Pfaffenwaldring 55, 70569 Stuttgart, Germany
[c] Lehrstuhl Anorganische Chemie I, Universität Bielefeld,
    Universitätsstr. 25, 33615 Bielefeld, Germany
    Supporting information for this article is available on the
   WWW under http://dx.doi.org/10.1002/ejic.200900516.

catalysts presumably differ in their structural and electronic properties from the catalytic species. Furthermore, the synthetic iron complexes might serve as models for polynuclear iron enzymes such as ferreascidin.[8] The results are reported below.

Results and Discussion

Synthesis and X-ray Crystallographic Studies

The synthesis of ligand precursors 5·HCl started with 2,6-pyridinedicarbaldehyde 1,[9] which was submitted to Horner–Emmons olefination in the presence of tetramethylguanidine in thf[10] to give the unsaturated ester 2a in 83% yield (Scheme 1). Wittig homologation[11] of 1 with triphenylphosphonium bromides 3a[12a] and 3b[12b] yielded the unsaturated ethyl dicarboxylates 2c,d. Derivatives 2a,c,d were catalytically hydrogenated[13] to the corresponding diesters 4, which were treated with aqueous HCl to give the hydrochlorides 5a·HCl and (5c,d)·HCl. As neither a ylide nor a phosphonate with methylene spacer between the phosphorus and the ester moiety was amenable, ligand precursor 5b·HCl was prepared by adapting a procedure by Jones.[14] 2,6-Dimethylpyridine (6) was deprotonated with nBuLi in Et$_2$O followed by treatment with homoallylic bromide to yield 2,6-dipentenylpyridine (7), which was submitted to ozonolysis in the presence of NaOH in MeOH/CH$_2$Cl$_2$ by utilizing a method by Marshall for the direct conversion of alkenes to methyl esters.[15] Final acid hydrolysis of the diester 4b gave the desired hydrochloride 5b·HCl in 89% yield. Single-crystal X-ray structure analyses of all ligand precursors 5a–d reveal that the pyridine N atom remains protonated throughout (Figure S1, Supporting Information).

In order to obtain the iron complexes, ligand hydrochlorides 5 were deprotonated with LiOH (2 equiv.) in MeOH and subsequently treated with anhydrous Fe(NO$_3$)$_3$ (1 equiv.). After removal of the solvent, complexes 8a–d were isolated as red solids in 68–90% yield (Scheme 2). Elemental analyses indicates that complexes 8 contain a trinuclear iron unit, presumably Fe$_3$(μ_3-O), and three pyridine-2,6-dicarboxylate ligands. According to ESI-MS spectra
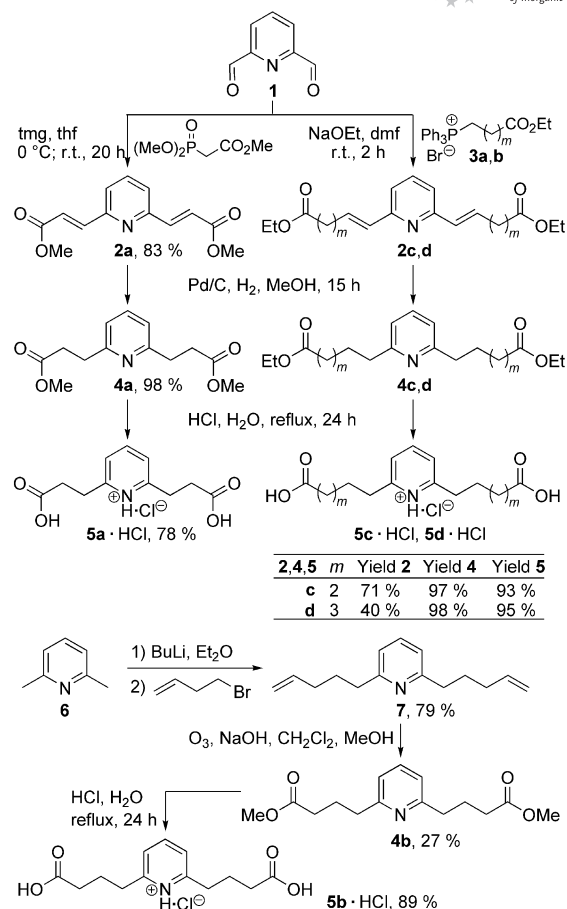
Scheme 1. Synthesis of ligand precursor 2,6-pyridinediacid hydrochlorides 5.

2,4,5	m	Yield 2	Yield 4	Yield 5
c	2	71%	97%	93%
d	3	40%	98%	95%

such [Fe$_3$O(L)$_3$]$^+$ species are also present in solution. For example, the ESI-MS spectrum of compound 8c derived from 5c reveals a charged species [Fe$_3$O(5c)$_3$]$^+$ at m/z = 1015. For the other complexes 8a,b and 8d, the corresponding peaks are found at m/z = 847, 931, and 1099, respectively.

Upon slow crystallization of a concentrated solution of 8a in water, however, a different complex [Fe$_4$O$_2$(5aH)$_2$Cl$_2$(H$_2$O)$_8$](NO$_3$)$_4$·3 H$_2$O (9) was formed. The redissolving

8	a	b	c	d
n	2	3	4	5
Yield [%]	68	74	78	90
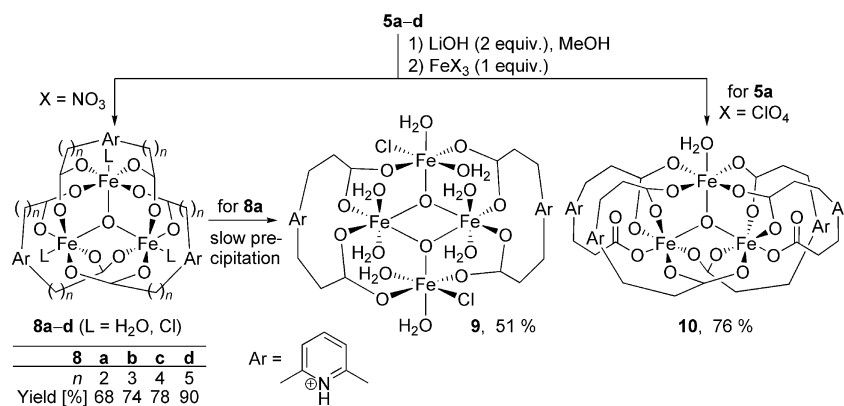
Scheme 2. Formation of the iron complexes 8–10.

of complex **9** in MeOH/H₂O (70:30) gave an ESI-MS spectrum identical to that of **8a**, which indicates that **9** is present only in the solid state. In contrast, when ligand **5a** was deprotonated with LiOH in MeOH followed by treatment with Fe(ClO₄)₃ (1 equiv.), complex **10** was obtained as a crystalline solid with the composition [Fe₃O(**5aH**)₄(H₂O)]-(ClO₄)₃·4H₂O, thus a trinuclear Fe₃(μ₃-O) unit is present together with four pyridine-2,6-dicarboxylate ligands. It should be noted that the Fe₃(μ₃-O) carboxylate triangle is a well-known structural motif, and in a recent study, Herchel and co-workers[5g] reported the formation of similar Fe₃(μ₃-O) complexes from pyrazolate-containing ligands.

Both the nitrate complex **9** and perchlorate complex **10** gave single crystals, which were suitable for X-ray crystal structure analysis (Figures 1 and 2). As shown in Figure 1, the nitrate complex **9** consists of a tetranuclear iron core with two Fe₃(μ₃-O) units. The pyridine N atoms are protonated and act as donors in an intermolecular hydrogen bond to one acceptor oxygen atom of a symmetry-related nitrate anion with a H1···O2S1 distance of 1.97 Å and a N1–H1···O2S1 angle of 169°. All carboxylate oxygen atoms O1, O2, O3, O4 and O1A, O2A, O3A, O4A are involved as ligands. The distances of the oxonium ion to the Fe2, Fe2A atoms are identical, and with a length of 1.993 Å, they are slightly longer than the distance to the Fe1, Fe1A ion (1.861 Å). The Fe2–Fe2A distance of 2.8898(7) Å is rather short, whereas Fe1–Fe2 is 3.4423(5) Å, as also documented by the Fe1–O1X–Fe2 and Fe2–O1X–Fe2A angles of 130.46(9)° and 96.83(7)°, respectively. While the Fe2, Fe2A atoms possess two axial water ligands, the Fe1, Fe1A atoms possess one axial and one equatorial H₂O ligand together with an equatorial chlorido ligand.
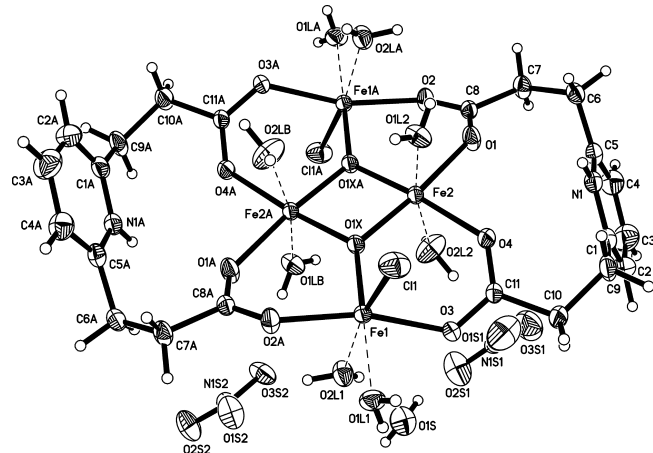

Figure 1. Solid-state structure of iron complex **9** with Fe₄O₂ core. The system crystallized with a half complex, two nitrate anions, and one solvent water molecule in the asymmetric unit.

In contrast, the solid-state structure of the perchlorate complex **10** consists of a central Fe₃(μ₃-O) unit with four pyridine ligands (Figure 2). The complex crystallizes with three perchlorate anions and three solvent water molecules, of which two are distributed on disordered positions. The perchlorate anions show a strong rotational behavior, indicated by large displacement parameters of the oxygen; some
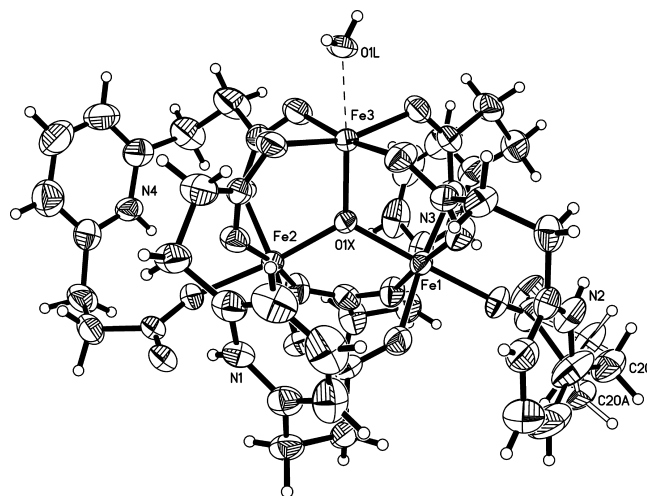

Figure 2. Solid-state structure of perchlorate complex **10**.

of them are fixed in discrete disordered positions. One side chain of a ligand is also disordered with a population ratio of 2:1. All carboxylate oxygen atoms are involved as ligands to the Fe atoms, with the exception of two, and act as acceptors in hydrogen-bond interactions with two protonated pyridine donors N1 and N3. The H1A···O14 and H3A···O8 distances (1.86 Å) as well as the N1–H1A···O14 and N3–H3A···O8 angles (178° and 165°), respectively, indicate a strong electrostatic interaction. N2–H2A and N4–H4A are donors to water and to a perchlorate oxygen atom.

Fe1 and Fe2 are equivalent and almost shielded by the pyridine ligands, and Fe3 bears a water ligand. The distances to the oxonium ion slightly differ: Fe1–O1X 1.956(5) Å, Fe2–O1X 1.915(5) Å, Fe3–O1X 1.888(5) Å. Both the Fe–Fe distances [3.3155(14)–3.3395(15) Å] and the Fe–OX1–Fe angles [119.2(2)–121(2)°] are comparable.

It should be emphasized that the pyridine units in complexes **9**, **10** and presumably in **8** remain protonated even if an excess amount of base was used in the preparation of the complexes. From the crystal structures of **9** and **10** and by considering previous results on tetranuclear Fe^III complexes with octadentate pyridine carboxylate ligands,[16] we assume that the sixth coordination sphere at the iron center in **8** might be occupied by water or a chlorido ligand.

EXAFS/XANES Studies

The local environment (including number, distances and kind of surrounding atoms) and the coordination geometry of the central Fe atom was observed with EXAFS and XANES spectroscopy, respectively. Iron complexes exhibit pre-edge features (prepeaks) in Fe-K edge spectra, which originate from a 1s→3d transition, whose energies and intensities strongly depend on spin state, oxidation state, and geometry.[17] In general, the total intensity of the transition shows an increase with decreasing coordination number because of the loss of inversion symmetry of the coordination sphere of the iron site.[18] For centrosymmetric iron sites, as in an octahedral coordination, the 1s→3d transition is par-

ity forbidden; however, a low intensity prepeak is visible in the experimental spectra, which results from quadrupole coupling.[19] The increasing prepeak intensity for non-centrosymmetric sites, e.g. tetrahedra, can be assigned to a metal 4p–3d mixing, which causes weakly allowed 1s→4p transitions.[20]

Figure 3 shows the XANES spectra of samples **8a–d**, together with the prepeak area. The prepeak intensity of approximately 0.06 found for all ligands is in accordance with an octahedrally coordinated iron(III) site.
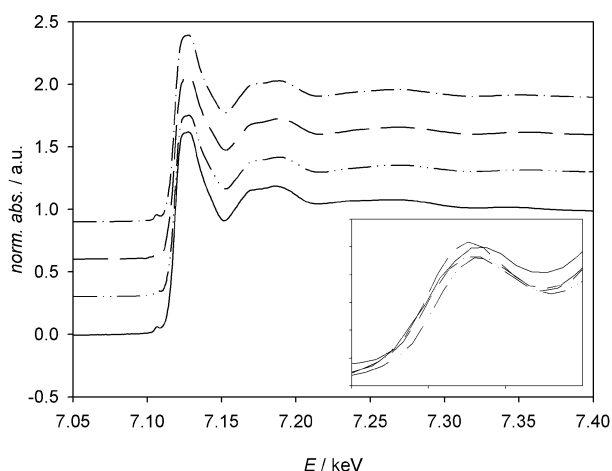

Figure 3. Experimental X-ray absorption (XANES) spectra of **8a** (solid line), **8b** (double-dotted dashed line), **8c** (long dashed line), **8d** (dotted dashed line). The samples were shifted for clarity. The inset shows the enlarged prepeak area.

Nevertheless, in former EXAFS studies of octahedral iron centers, a slightly lower intensity was found.[21] Additionally, the absence of a signal at ca. 7.132 keV after the first XANES resonance (white line) in the spectra presented here suggests that only a distorted octahedral coordination geometry is present.[22] All samples exhibit the same edge

position, i.e. they possess the same oxidation state of +3. The numeric results obtained by fitting the Fourier filtered EXAFS spectra of the Fe–O, Fe–C, and Fe–Fe shell (Figures S2 and S3, Supporting Information) with theoretical models are summarized in Table 1.

As the coordination numbers and distances of the Fe–O shells of **8a–d** investigated by EXAFS are identical to those of the XRD-characterized structure **10** within error (Entries 1, 4, 7, 10, and 13), an octahedral coordination by oxygen can be unambiguously concluded for all samples. Furthermore, similar Debye–Waller factors indicate a comparable degree of disorder. Owing to an additional carboxylate ligand in structure **10**, the carbon coordination number is not comparable to **8a–d**. Compounds **8a–d** show similar carbon coordination numbers within error (Entries 5, 8, 11, and 14), but it must be kept in mind that the fit results for carbon, which is a light backscatterer, should be only used in a comparative way, and the absolute values of the coordination number are not reliable.[23] Nevertheless, the Fe–C distances are in good accordance with those of the crystalline reference **10** (Entry 2). No chlorine shell could be adjusted to any of the samples.

The Fe–Fe coordination number of all samples (Entries 3, 6, 9, 12, and 15) corresponds to a trinuclear Fe_3O core, which exhibits an average iron coordination number of two. Since no higher aggregates than trinuclear iron frameworks could be detected by mass spectrometry, the high iron coordination number of 2.9 in **8b** (Entry 9) can be explained by a large degree of disorder, which leads to a large Debye–Waller factor, whose strong correlation with the coordination number in turn increases the latter. However, small amounts of higher aggregates below the detection limit of EXAFS spectroscopy can still be present.

The EXAFS analysis shows that all investigated samples are highly similar to the well-defined trinuclear structure **10**. Therefore, a Fe_3O core can be concluded for all samples, and the detected small differences in the EXAFS results are caused by disorder effects.

Table 1. Structural parameters obtained by fitting the experimental EXAFS data.

Entry	Sample	Bs	N(Bs)[a]	R(Bs)[b] [Å]	σ[c] [Å]	Distance for filter process[d] [Å]	E_f[e] [eV]
1	**10** (XRD)	Fe–O	6	2.01			
2		Fe–C	4.7	3.02			
3		Fe–Fe	2	3.34			
4	**8a**	Fe–O	6.0 ± 0.6	2.01 ± 0.02	0.092 ± 0.009	1.0–2.1	4.32
5		Fe–C	4[f]	3.01 ± 0.03	0.055 ± 0.006	2.55–3.0	−7.78
6		Fe–Fe	2[f]	3.37 ± 0.03	0.074 ± 0.014	3.0–3.4	−4.29
7	**8b**	Fe–O	6.4 ± 0.6	2.02 ± 0.02	0.087 ± 0.009	−2.1	2.39
8		Fe–C	3.4 ± 0.7	2.98 ± 0.03	0.055 ± 0.006	2.5–2.9	−7.33
9		Fe–Fe	2.9 ± 0.6	3.35 ± 0.03	0.095 ± 0.019	3.0–3.5	−4.39
10	**8c**	Fe–O	6.0 ± 0.6	2.02 ± 0.02	0.081 ± 0.008	1.1–2.1	0.68
11		Fe–C	2.9 ± 0.6	3.02 ± 0.03	0.039 ± 0.004	2.6–3.0	−9.76
12		Fe–Fe	2.4 ± 0.5	3.34 ± 0.03	0.084 ± 0.016	3.0–3.4	−5.14
13	**8d**	Fe–O	6.3 ± 0.6	2.01 ± 0.02	0.089 ± 0.009	−2.1	3.05
14		Fe–C	3.4 ± 0.7	2.98 ± 0.03	0.063 ± 0.006	2.5–2.9	−7.14
15		Fe–Fe	2.0 ± 0.4	3.35 ± 0.03	0.081 ± 0.016	3.0–3.4	−5.11

[a] Number of backscattering neighbor atoms. [b] Distance of backscattering atoms. [c] Debye–Waller factor (mean-square displacement). [d] Distance range used in the Fourier filtering process. [e] Fermi energy: accounts for energy shift between experimental and theoretical EXAFS functions. [f] Value was fixed to the expected structure in order to achieve a sound determination of the amplitude reduction factor.

Mössbauer Studies of Complexes 8a and 10

The Mössbauer spectrum of complex **8a** at 4.2 K (Figure 4) displays a quadrupole doublet with isomer shift $\delta = (0.525 \pm 0.001)$ mm s^{-1}, quadrupole splitting $|\Delta E_Q| = (0.652 \pm 0.001)$ mm s^{-1}, and line width $\Gamma = 0.60$ mm s^{-1}, which indicates a high-spin Fe^{III} complex.[24] The isomeric shift resembles those of other Fe$_3$(μ_3-O) complexes, such as [Fe$_3$(μ_3-O)(O$_2$CPh)$_6$(EtOH)$_2$(N$_3$)]·2.4EtOH, which shows a doublet at $\delta = 0.537$ mm s^{-1} with $|\Delta E_Q| = 0.425$ mm s^{-1} at 4.2 K.[25]
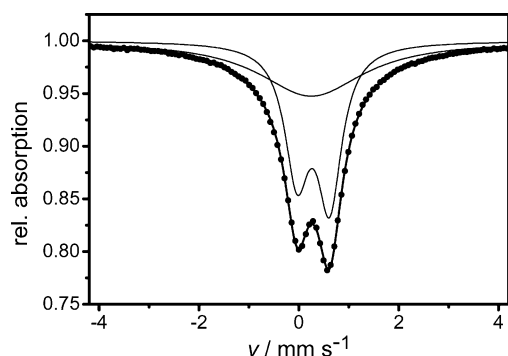

Figure 4. ^{57}Fe Mössbauer spectrum of **8a** at 4.2 K. The dots are the experimental data points and the thick solid line is the fitted spectrum, which corresponds to the sum of an asymmetric quadrupole doublet (parameters given in the text) and a singlet ($\delta = 0.485 \pm 0.005$ mm s^{-1}; $\Gamma = 2.56$ mm s^{-1}). As a result of spin relaxation, the spectrum shows a wide shoulder and hence a singlet is necessary to obtain a good fit.

In contrast, the Mössbauer data of several trinuclear iron complexes reported reveals the presence of mixed valence complexes. For example, [Fe$_3$(μ_3-O)(OAc)$_6$(3-Et-py)$_3$]·0.5toluene displays two doublets at $\delta = 1.242$ mm s^{-1} and 0.531 mm s^{-1} with $|\Delta E_Q| = 1.039$ mm s^{-1} and 1.051 mm s^{-1}, respectively, which corresponds to a Fe^{II}/Fe^{III} ratio of 34:66.[26] Coucouvanis observed two doublets at $\delta = 1.29$ mm s^{-1} and 0.48 mm s^{-1} with $|\Delta E_Q| = 1.89$ mm s^{-1} and 0.71 mm s^{-1}, respectively, for [Fe$_3$(μ_3-O)(OAc)$_7$(H$_2$O)]NEt$_4$, which corresponds to a Fe^{II}/Fe^{III} ratio of 1:2.[5u]

At room temperature, complex **8a** displays a quadrupole doublet with $\delta = (0.410 \pm 0.001)$ mm s^{-1}, $|\Delta E_Q| = (0.574 \pm 0.001)$ mm s^{-1}, and $\Gamma = 0.41$ mm s^{-1} (Figure S4, Supporting Information). The broadening of the line width and the increase in quadrupole splitting at 4.2 K indicates that the Fe sites in the complex are not perfectly equivalent and apparently arise because of the onset of spin relaxation effects.[27] The decrease in δ on raising the temperature is probably due to the second-order Doppler effect.[28] The dissolution of **8a** in a mixture of zinc, acetic acid, and pyridine under N$_2$ gas (i.e. active catalyst) resulted in a high-spin Fe^{II} complex with a doublet at $\delta = (1.184 \pm 0.002)$ mm s^{-1} and $|\Delta E_Q| = (3.392 \pm 0.003)$ mm s^{-1}, where the large quadrupole splitting reflects the strong valence-electron-induced asymmetry contribution. Under Gif-type conditions (active catalyst under O$_2$ gas), a second high-spin Fe^{III} species appears as a doublet at $\delta = (0.54 \pm 0.01)$ mm s^{-1} with $|\Delta E_Q| = (1.04 \pm 0.01)$ mm s^{-1} (see

Supporting Information). This may be a hint that part of the catalyst is modified during the reaction. Presumably, a mononuclear [Fe(OAc)$_m$(py)$_n$] species is formed, as was suggested by Stavropoulos for Gif-type chemistry.[5o] No magnetic splittings are observed, i.e. they are either nonexistent (diamagnetism) or the magnetic fluctuations are much faster than the Mössbauer time window (141 ns).

The ^{57}Fe Mössbauer spectrum of **10** at 80 K (Figure 5) consists of two asymmetric absorption lines indicative of more than one iron species present in **10**. The spectrum can be fitted with two quadrupole doublets of different intensities. The strong overlap of the two quadrupole doublets does not allow a unique solution of the experimental data. However, the parameters for the isomer shifts δ and the quadrupole splittings $|\Delta E_Q|$ do not vary significantly with slight changes in the peak area ratio. A good representative fit is provided in Figure 5, with the following values: quadrupole doublet 1 (64%) $\delta_1 = (0.51 \pm 0.01)$ mm s^{-1}, $|\Delta E_Q| = (0.60 \pm 0.03)$ mm s^{-1}, $\Gamma = (0.41 \pm 0.02)$ mm s^{-1}; quadrupole doublet 2 (36%) $\delta_1 = (0.54 \pm 0.01)$ mm s^{-1}, $|\Delta E_Q| = (1.03 \pm 0.03)$ mm s^{-1}, $\Gamma = (0.32 \pm 0.02)$ mm s^{-1}.
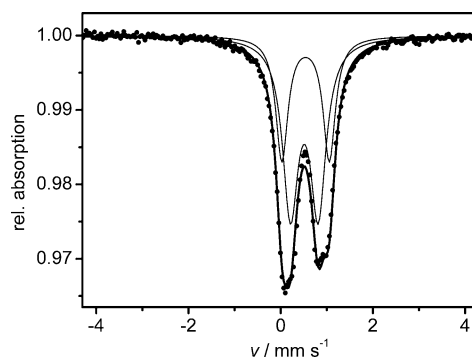

Figure 5. ^{57}Fe Mössbauer spectrum of **10** at 80 K. The dots are the experimental data points, the thin solid lines are the two subspectra with the parameters given in the text. The thick solid line corresponds to the sum of the two subspectra.

The isomer shift values are consistent with Fe^{III} high spin ($S_i = 5/2$) with O- and N-donor ligands.[29] The intensity ratio 2:1 corresponds to the molecular structure of **10** in which Fe1 and Fe2 have similar environments (see Figure 2). The lack of equivalence between the three iron sites in **10** is likely to be the cause of the unusual electronic properties. A similar behavior for a bis(trinuclear) Fe^{III} cluster containing two Fe$_3$O units was recently reported.[27]

Magnetic Studies

Magnetic susceptibility data of complex **10** was measured on a microcrystalline sample in the temperature range 2–290 K with an applied field of 1 T. The effective magnetic moment, μ_{eff}, decreases steadily from 5.94 μ_B at 290 K to 1.90 μ_B at 2 K, which is indicative of moderate antiferromagnetic interactions yielding a $S_t = 1/2$ spin ground state.

The Mössbauer spectrum clearly demonstrates the existence of high-spin ferric ions with $S_i = 5/2$. Thus, the magnetic properties of **10** have been analyzed by using the ap-

propriate spin Hamiltonian (Equation 1) for three coupled spins $S_i = 5/2$ (coupling scheme: inset Figure 6a)[30] including the isotropic Heisenberg–Dirac–van-Vleck (HDvV) exchange Hamiltonian and the single-ion Zeeman interaction by full-matrix diagonalization.

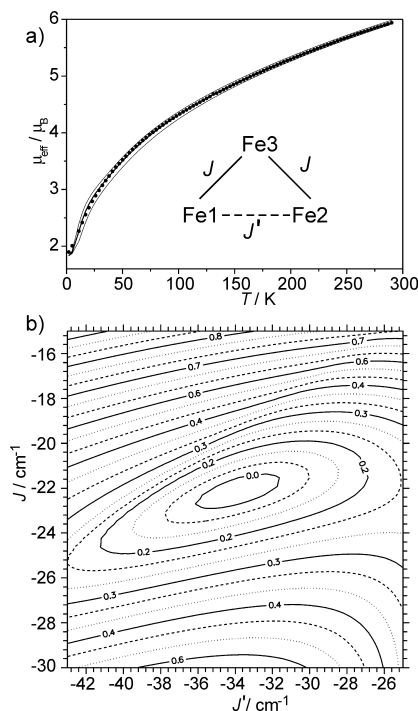$$H = 2J(S_1S_3 + S_2S_3) - 2J'S_1S_2 + \sum_{i=1}^{3} \mu_B S_i g_i B \qquad (1)$$

Figure 6. (a) Temperature-dependence of the effective magnetic moment, μ_{eff}, of **10** at 1 T. The thick solid line is a simulation of the experimental data to the spin-Hamiltonian (Equation 1) with $J = -22.1$ cm^{-1}, $J' = -33.8$ cm^{-1}, $g_i = 2.00$ (fixed), and a paramagnetic impurity ($S = 5/2$) of 1.6%. The thin solid lines correspond to simulations with the same parameter set but with $J = -21.5$ cm^{-1} or $J = -22.7$ cm^{-1} to demonstrate the accuracy of the coupling constants provided. Inset: coupling scheme for **10**. (b) Two-dimensional contour projection of the relative error surface for varying J and J'. The surface was calculated with $g_i = 2.00$ and with a paramagnetic impurity ($S = 5/2$) of 1.6%.

Zero-field splitting has been neglected as it does not contribute significantly to the experimentally observed antiferromagnetic interactions with a $S_t = 1/2$ spin ground state. The isotropic g values were fixed to 2.00. The fitting of J and J' gave a good reproduction of the experimental data with $J = -22.1$ cm^{-1} and $J' = -33.8$ cm^{-1}, including 1.6% of a $S = 5/2$ paramagnetic impurity (Figure 6a). To determine if this is a unique fit, a search of the (J, J') parameter space was performed by keeping $g = 2.00$ and a paramagnetic impurity ($S = 5/2$) of 1.6% fixed. In Figure 6b, a two-dimensional contour projection of the relative error surface for varying J and J' is shown.

Only the region of smallest relative error is presented. It can be concluded that the parameters given above correspond to a well-defined global minimum in the parameter space for this system. The value of J is slightly better de-

fined than the value for J'. This procedure allows us to estimate the error on the quoted values of J and J' as approximately ± 0.6 cm^{-1} and ± 1.0 cm^{-1}, respectively; these errors represent very conservative estimates. Figure 6a exhibits simulations with $J = -21.5$ cm^{-1} and $J = -22.7$ cm^{-1} as thin lines, which demonstrates that these simulations do not give as good reproductions of the experimental values as $J = -22.1$ cm^{-1}. These values are in the typical region found in basic iron carboxylates like **5**.[31]

EPR Studies

In order to characterize complex **10** further, an X-band EPR study was carried out. Figure 7 shows an EPR spectrum that is dominated by an intense, sharp peak at $g_\parallel \approx 2.0$ with a broad (several kG wide) peak towards higher fields with zero-crossing near $g_{iso} \approx 1.8$ and a very weak peak at $g = 4.3$.
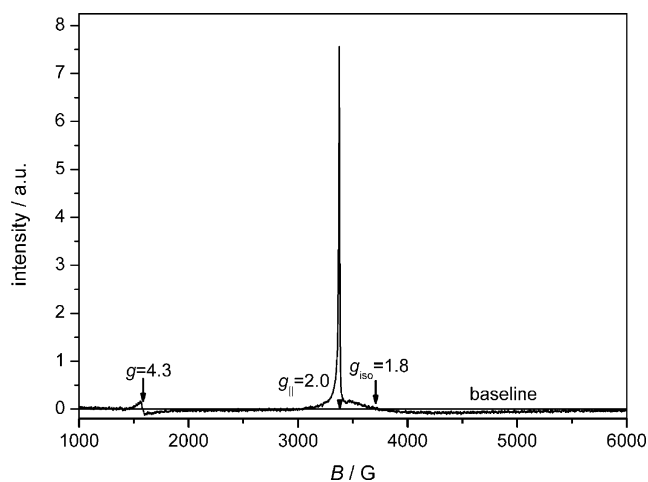

Figure 7. EPR spectrum of compound **10** measured at 4 K.

The Mössbauer studies clearly show that the individual Fe^{III} ions are in a high spin state ($S_i = 5/2$), while antiferromagnetic behavior is established by the magnetic studies. This apparent contradiction is explained by a coupling between the three Fe^{III} ions, which yields a total spin of $S = 1/2$ for the cluster.

To clarify whether the observed signal represents the majority of iron or whether it sees a spurious effect, the EPR signal intensity was compared to that of a reference sample (ultramarine blue diluted by KCl, $g = 2.03$, $S = 1/2$, spin concentration [std] $= 7.7 \times 10^{-6}$ mol L^{-1}), and the spin concentration was calculated by using Equation (2).[32]

$$[X] = \frac{A_x (g_{std})^2 [S(S+1)]_{std}}{A_{std} (g_x)^2 [S(S+1)]_x} [std] \qquad (2)$$

[X] and [std] are the unknown spin concentration of the sample and the known spin concentration of the standard, respectively. The parameters A, S and g are the measured intensities (double integrals of the derivative spectra), the electron spin quantum numbers, and the g factors. The important experimental parameters of temperature, amplifi-

cation, scan time, modulation amplitude, and power were omitted in Equation (2) since they are identical for both sample and standard. The isotropic value, $g_{iso} = (2g_\perp + g_\parallel)/3 \approx 1.8$, was used for g_X.

By assuming that the Fe^{III} ions are independent and carry a $S = 5/2$ spin, a spin concentration of 1.4×10^{-3} mol L^{-1} was calculated, which would represent only ca. 7% of the iron concentration of $c_{Fe(III)} = 2.1 \times 10^{-2}$ mol L^{-1} in the sample. On this basis, the observed signal could only account for a very small fraction of the iron atoms, the remainder would have to be in diamagnetic states or in paramagnetic states that are EPR-silent. Alternatively, the signal represents the spin concentration of a coupled $S = 1/2$ state of a triatomic iron cluster and is calculated to be 1.7×10^{-2} mol L^{-1}, which corresponds to 0.8 spins per iron ion or, since there are three iron ions in a cluster, 2.4 spins per cluster. In this case, the signal seems to be larger than expected for the nominal iron content, but it should be noted that the determination of absolute spin concentrations is often rather difficult.[32] The EPR experiments are thus in agreement with the magnetic studies, which demonstrate that coupling of the Fe^{III} ions in the clusters leads to an $S = 1/2$ ground state. This is also very compatible with $g_{iso} \approx 1.8$.

The line shape of the signal is very unusual, but an almost identical feature was reported recently for an oxonuclear complex with the same Fe$_3$O metal core.[27] It was found that the strong asymmetric signal is compatible with a system possessing an $S = 1/2$ ground state. It was assigned to a near-axial system with well-defined $g_\parallel = 2.00$ and $g_\perp \approx 1.70$ values, with a high g strain.

When the temperature is raised, the intensities of the peak at $g_{iso} \approx 1.8$ and at $g = 4.3$ decrease (Figure 8). The latter has the typical shape of an EPR line that is slightly broadened by anisotropy and is attributed to the high-spin $S = 5/2$ Fe^{III} impurity mentioned in the magnetic studies. Its intensity follows roughly the Curie law.[27]

The intensity of the signal at $g_{iso} \approx 1.8$ also follows the Curie law, although it seems to disappear much faster. The additional loss of amplitude must be caused by relaxation,
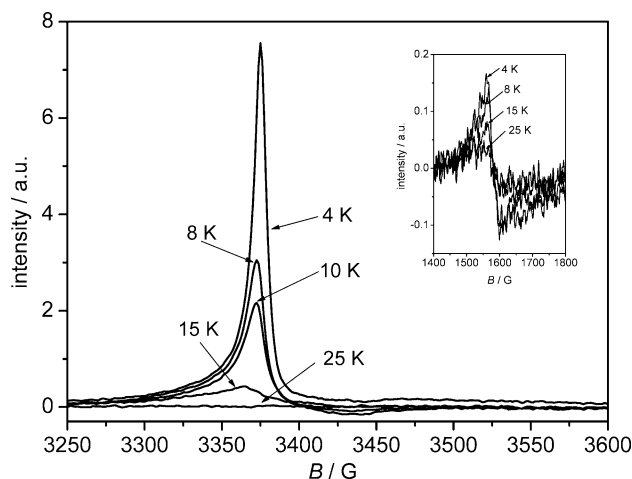

Figure 8. EPR spectra of compound **10** between 4 and 25 K for $g_{iso} \approx 1.8$. The inset shows the temperature dependence of the peak at $g = 4.3$.

which increases rapidly with temperature. Relaxation broadens the lines but does not affect their intensities.

In the magnetic studies, the antiferromagnetic coupling constants are determined to be $J = -22.1$ cm^{-1} and $J' = -33.8$ cm^{-1}, which corresponds to $J \approx 33$ K and $J' \approx 51$ K, respectively, in temperature units. When the temperature exceeds these critical temperatures, the coupling in the cluster is overcome by thermal fluctuations, which causes fast relaxation and the loss of amplitude.

In summary, the EPR and Mössbauer spectra of complex **10** agree well with the data published by Boudalis and Sanakis for an octanuclear picolinate complex containing two FeO units.[27]
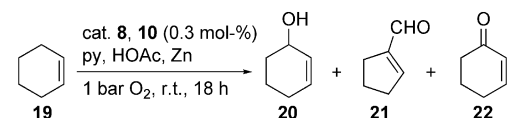
Oxidation Catalysis

The nitrate complexes **8a**–**d**, **9**, and the perchlorate complex **10** were employed in catalytic aerobic Gif-type oxidations using adamantane **11**, cyclohexene **19**, and α-pinene **23** in order to assess the catalytic properties towards different C–H bonds (Tables 2, 3, and 4).

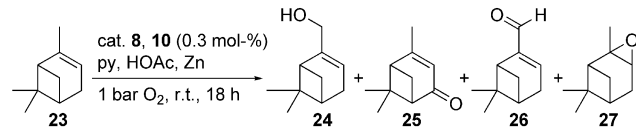Table 2. Catalytic oxidation of adamantane **11** under Gif-type conditions.[a]

Entry	Catalyst	Yield [%]				(13+14):12 (C^2:C^3)	TON
		12	**13**	**14**	Total		
1	**8a**	1.5	0.5	3.6	5.6	48:52	15
2	**8b**	1.2	0.4	3.7	5.5	53:47	21
3	**8c**	0.6	0.2	1.1	1.9	42:58	7
4	**8d**	0.5	0.2	1.1	1.8	46:54	6
5	**9**	2.0	1.0	5.9	8.9	53:47	29
6	**10**	2.0	1.2	2.6	5.8	39:61	19
7	[Fe(OAc)$_2$(py)$_4$][b]	0.6	1.3	11.3		32:68	3
8	[Fe$_2$(μ-(OH$_2$))(OAc)$_5$(py)$_2$]NEt$_4$[c]	1.9	0.8	10.0		70:30	7
9	[Fe$_3$(μ$_3$-O)(OAc)$_6$(py)$_3$][d]	1.4	2.0	8.2		41:59	13
10	[Fe$_3$(μ$_3$-O)(OAc)$_7$(OH$_2$)]NEt$_4$[c]	0.9	0.9	8.5		50:50	6
11	[Fe$_4$(μ$_3$-O)$_2$(OAc)$_6$(py)$_4$]Cl$_2$[c]	1.0	0.8	8.1		56:44	7

[a] Adamantylpyridines **15**–**18** were obtained in 4.4–7.7% yield in a ratio (**15**+**16**):(**17**+**18**) ≥ 91:9 (see Supporting Information). They were not considered in the calculation of TON. TONs were calculated according to ref.[34] [b] See ref.[5v,5w] data from ref.[5w] [c] See ref.[5u] [d] See ref.[2b]

Table 3. Catalytic oxidation of cyclohexene **19** under Gif-type conditions.

| Catalyst	Yield [%]			20:22	TON[a]
	20	**21**	**22**		
8a	0.3	1.6	5.3	5:95	39
8b	0.5	2.0	5.7	4:96	48
8c	0.2	1.9	5.6	3:97	42
8d	0.3	1.9	5.8	9:91	43
10	0.3	1.9	6.3	5:95	44
[Fe$_3$(μ_3-O)(OAc)$_6$(py)$_3$][b]	—[b]	1.3	1.1	–	—[c]

[a] TON was calculated without the yield of **21**, which is formed in a separate autoxidation process. [b] See ref.,[2b] cyclohexenol **20** was not observed. [c] The catalyst was prepared in situ. For details see ref.[2b]

Table 4. Catalytic oxidation of α-pinene **23** under Gif-type conditions.

Catalyst	Yield [%]				(24+25+26):27 (C^1:C^2)	24+26):25	TON[a]
	24	**25**	**26**	**27**			
8a	0.1	2.4	0.5	0.7	81:19	20:80	10
8b	0.2	1.9	0.5	0.5	84:16	27:73	8
8c	0.1	1.6	0.5	0.5	81:19	27:73	6
8d	0.1	1.1	0.5	0.7	71:29	35:65	6
10	0.1	2.4	0.4	0.7	81:19	17:83	10

[a] For calculation see ref.[34]

Under Gif-type conditions adamantane **11** was oxidized to give products **12**–**14**, and as side products the adamantyl-pyridines **15**–**18** could be detected (Scheme 3). Their formation probably proceeds via adamantyl radicals, which attack pyridine preferably at positions 2 and 4.[5v,33]
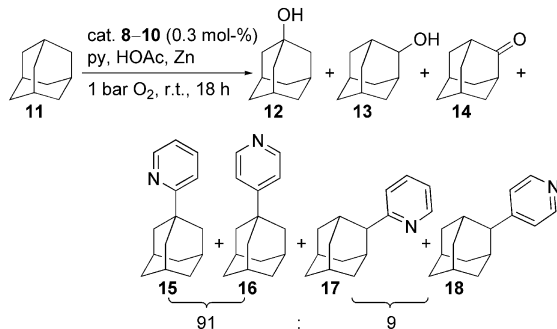
Scheme 3. Gif-type oxidation of adamantane **11**.

The adamantylpyridines **15**–**18** were formed in total yields of 4.4–7.7% with the lowest percentage of 4.4% in the case of perchlorate complex **10** (Supporting Information). For all catalysts **8**–**10**, the formation of the C^3

products **15**, **16** is favored as compared to the C^2 products **17**, **18**, and the ratios found resemble those reported in the literature (93:7).[33a]

As can be seen from Table 2, the turnover numbers[34] of complexes **8a**,**b** and **10** in the oxidation of adamantane **11** resemble those of complexes in the literature,[2a,2b,5u–5w] whereas the reactivity decreases for complexes **8c** and **8d** with longer alkyl chains between the pyridine and carboxylate units. For all complexes, ketone **14** was the favored product, but varying ratios of alcohols **12** and **13** were found.

Generally, with regard to oxidation products **12**–**14**, oxidation of the tertiary C–H bond (C^3) by complexes **8**, **10** was slightly preferred (Entries 1, 3, 4, 6), whereas complex **9** gave a reversed ratio of C^2:C^3 = 53:47 (Entry 5). The formation of the tertiary adamantyl radical is much more dominant than that of the secondary radical, and thus, considering both oxidation products **12**–**14** and adamantylpyridines **15**–**18**, C^2/C^3 ratios of 23:77 to 8:92 results. It should be noted that the di-, tri-, and tetranuclear iron complexes described by Coucouvanis[5u] and Barton,[2b] as well as the mononuclear complex described by Stavropoulos,[5v,5w] yield a larger amount of the ketone **14** relative to that formed by iron complexes **8a**–**d**.

Under Gif-type conditions, cyclohexene **19** was oxidized to cyclohexenol **20** and cyclohexenone **22**. Additionally, the autoxidation product, cyclopentenecarbaldehyde **21**, was obtained (Table 3).

The fact that no cyclohexene oxide was observed may be taken as further evidence of a radical mechanism favoring allylic oxidation. However, this hypothesis has to be treated with great care as will be discussed for α-pinene oxidations (see below). Turnover numbers between 39 and 48 were observed; complex **8b** as catalyst gives a higher TON relative to the complexes with other chain lengths in this series. For the iron perchlorate complex **10**, similar results were obtained. Regardless of the tether lengths, the chemoselectivity is in the same range. The results agree with Barton's report on Fe$_3$(μ_3-O)(OAc)$_6$(py)$_3$,[2b] although he did not observe cyclohexenol **20**.

The oxidation of α-pinene **23** yielded myrtenol **24**, verbenone **25**, myrtenal **26**, and α-pinene oxide **27**, with verbenone **25** as the major product (Table 4).

Irrespective of the catalysts **8**, **10**, allylic oxidation is favored over epoxidation with a ratio of 84:16 and takes place preferably at the secondary C–H bond; C^2:C^1 ratios of 65:35 to 83:17 were obtained. The formation of epoxide **27** indicates that, at least under Gif-type conditions, a nonradical mechanism via an Fe^V=O species cannot completely ruled out.[33b,33c]

Conclusions

Starting from a common precursor **1**, a series of trinuclear Fe$_3$(μ_3-O) complexes **8a**–**d** and **10** was prepared, which contains 2,6-diacylpyridine ligands with different tether lengths between the carboxyl and pyridine moiety. Surpris-

ingly, the tether lengths do not influence the nuclearity. Furthermore, the pyridine nitrogen atom is not involved in bonding to the iron centers, as was shown by the X-ray crystal structure analysis of **10**.[35] Spectroscopic and analytical data reveal that both in solution and in the solid state the trinuclear $Fe_3(\mu_3\text{-O})$ species are favored. A combined XANES/EXAFS study provides sound information about the local structure around the iron center in the samples **8a–d**. Prepeak analysis of the XANES spectra unambiguously proves an octahedral nearest neighbor coordination, which is supported by evaluation of the EXAFS data. Moreover, a trinuclear Fe_3O core is concluded from the EXAFS spectra for all complexes **8a–d**, which differ only by the degree of disorder in the individual Fe_3 framework. However, under slow equilibration conditions, tetranuclear Fe_2O_4 species may form as well, as is exemplified by crystalline complex **9**. Furthermore, in Gif-type catalytic aerobic oxidations, complexes **8a–d** and **10** are not the actual catalysts. Presumably, the trinuclear complexes break up into mononuclear iron complexes according to the freeze quench Mössbauer (Supporting Information)[36a] and NIS data.[36b,36c] With respect to the catalytic properties, it should be noted that "precatalysts" **8a,b** and **10** with short tether lengths of the ligands give slightly better turnover numbers and selectivities in C–H oxidation relative to complexes **8c,d** with longer tethers. When cyclohexene **19** and α-pinene **23** were employed as substrates, a strong preference for allylic oxidation over epoxidation was found.

Besides the Gif oxidation chemistry, trinuclear $Fe_3(\mu_3\text{-O})$ complex **10** may be a relevant model for ferritin mineralization. Högdom and Nordlund reported the X-ray crystal structure of a protein–carboxylate–coordinated, oxo-centered, tri-nuclear iron cluster, which is formed on the surface of the ribonucleotide reductase R2 protein from *Corynebacterium ammoniagenes* during Fe^{2+} uptake of the protein from solution.[37] This natural iron complex bears some structural resemblance to complex **10**, i.e. the central $Fe_3(\mu_3\text{-O})$ unit, the bridging carboxylate ligands, and the axial coordination site is occupied by a water molecule.

Experimental Section

General: All reactions were carried out under standard Schlenk techniques by using inert atmosphere. Melting points were determined on a Büchi SMP 20 and are uncorrected. NMR spectra were recorded on a Bruker Avance 300 or a Bruker Avance 500 spectrometer (^{1}H: 300 or 500 MHz, ^{13}C: 75 or 125 MHz) with tms as internal standard. Signal assignments are based on DEPT experiments. IR spectra were recorded on a Bruker Vector 22 FTIR spectrometer. Mass spectrometry was performed on a Bruker Daltonics micrOTOF_Q spectrometer. Thick film gas chromatography was performed on a Carlo Erba Strumentazione Fractovap 4160 and GC on a Hewlett–Packard HP 6890 instrument. UV/Vis spectra were measured in a two-beam photometer Cary 100 Scan (Varian) spectrometer. Chromatography was performed on silica gel 60 (230–400 mesh) (Macherey–Nagel). Commercial reagents were used without further purification. MeOH was distilled from $Mg(OMe)_2$ under N_2. Pyridine was distilled from CaH_2, thf was

distilled from Na under N_2. Cyclohexene was freshly distilled prior to use. The following compounds were prepared as described in the literature: **1**,[9] **3a,b**,[12] and **15–18**.[33a]

Methyl (2E)-3-{6-[(1E)-3-Methoxy-3-oxoprop-1-enyl]pyridin-2-yl}-acrylate (2a): A solution of trimethylphosphonoacetate (19.5 mL, 21.9 g, 0.12 mol) and tetramethylguanidine (16.2 mL, 13.8 g, 0.12 mol) in thf (210 mL) was added dropwise to a solution of aldehyde **1** (6.49 g, 48.1 mmol) in absolute thf (50 mL) at 0 °C. After stirring for 4 h, the mixture was warmed to room temperature and stirred for a further 20 h. The solvent was removed under reduced pressure, and the residue dissolved in $CHCl_3$ (100 mL). The organic layer was washed with H_2O (2 × 100 mL) and brine (100 mL), dried ($MgSO_4$), and concentrated under vacuum. The residue was recrystallized from $CHCl_3$ to give **2a** as a colorless solid (9.923 g, 40.133 mmol, 83%). M.p. 173 °C. FTIR (ATR): $\tilde{v}$ = 3416 (w), 3074 (w), 3020 (w), 2961 (m), 2844 (w), 1722 (vs), 1647 (s), 1578 (s), 1432 (s), 1325 (s), 1315 (s), 1301 (vs), 1218 (vs), 1193 (s), 1146 (vs), 1066 (m), 1016 (m), 992 (s), 974 (vs), 904 (m), 878 (m), 805 (s), 786 (m), 742 (m), 731 (m), 694 (m), 601 (s) cm^{-1}. ^{1}H NMR (500 MHz, CDCl$_3$): δ = 3.84 (s, 6 H, OCH$_3$), 7.04 (d, J = 15.6 Hz, 2 H, 2-H), 7.37 (d, J = 7.7 Hz, 2 H, *m*-H), 7.68 (d, J = 15.6 Hz, 2 H, 1-H), 7.74 (t, J = 7.7 Hz, 1 H, *p*-H) ppm. ^{13}C NMR (125 MHz, CDCl$_3$): δ = 51.9 (OCH$_3$), 122.8 (*m*-CH), 124.7 (C-2), 137.6 (*p*-CH), 142.9 (C-1), 153.0 (*o*-CH), 167.1 (C=O) ppm. MS (EI): m/z (%) = 247.1 (100) [M$^+$], 216 (82), 156 (96), 131 (76), 102 (21), 77 (9). C$_{13}$H$_{13}$NO$_4$ (247.25): calcd. C 63.15, H 5.30, N 5.66; found C 62.94, H 5.31, N 5.56.

2,6-Dipent-4-enylpyridine (7): A 1.6 M solution of *n*BuLi (24.5 mL, 39.2 mmol) in hexane was added dropwise over 12 min to a solution of **6** (2.2 mL, 2.00 g, 18.7 mmol) in Et$_2$O (10 mL) at 0 °C, and the reaction mixture stirred for 20 min. A solution of 4-bromobutene (4.2 mL, 5.55 g, 41.1 mmol) in Et$_2$O (4 mL) was added dropwise over 20 min, and after stirring for 5 h, the mixture was poured into H$_2$O (50 mL). The layers were separated, and the aqueous layer was extracted with Et$_2$O (3 × 30 mL). The combined organic layers were dried (MgSO$_4$) and concentrated under reduced pressure, and the residue was chromatographed on SiO$_2$ with hexanes/EtOAc (10:1) to yield in a first fraction (R_f = 0.57) **7** as a colorless liquid (1.04 g, 4.83 mmol, 26%) and in a second fraction (R_f = 0.37) 2-methyl-6-(pent-4-enyl)pyridine (1.78 g, 11.0 mmol, 59%). Following this procedure, the latter was converted into **6** (91%). Thus, **6** was isolated in a total yield of 79%. FTIR (ATR): $\tilde{v}$ = 3075 (w), 2976 (w), 2925 (m), 2858 (w), 1640 (w), 1589 (s), 1576 (s), 1455 (s), 1218 (w), 1154 (w), 1086 (w), 991 (m), 908 (s), 852 (w), 798 (m), 765 (m), 749 (m) cm^{-1}. ^{1}H NMR (500 MHz, CDCl$_3$): δ = 1.78–1.84 (m, 4 H, 2-H), 2.09–2.15 (m, 4 H, 3-H), 2.74–2.78 (m, 4 H, 1-H), 4.96 (ddt, J = 10.3, J = 2.1, J = 1.3 Hz, 2 H, 5-H$_{trans}$), 5.02 (ddt, J = 17.1, J = 2.1, J = 1.5 Hz, 2 H, 5-H$_{cis}$), 5.85 (ddt, J = 17.1, J = 10.3, J = 6.7 Hz, 2 H, 4-H), 6.95 (d, J = 7.8 Hz, 2 H, *m*-H), 7.48 (t, J = 7.8 Hz, 2 H, *p*-H) ppm. ^{13}C NMR (125 MHz, CDCl$_3$): δ = 29.3 (C-2), 33.5 (C-3), 37.9 (C-1), 114.7 (C-5), 119.8 (*m*-CH), 136.4 (C-4), 138.9 (*p*-CH), 161.6 (*o*-C) ppm. MS (ESI): m/z = 238.2 [M + Na]$^+$, 230.2, 216.2 [M + H]$^+$, 174.1. HRMS (ESI): calcd. for C$_{15}$H$_{22}$N 216.1747; found 216.1742.

2-Methyl-6-(pent-4-enyl)pyridine: FTIR (ATR): $\tilde{v}$ = 3065 (w), 2976 (w), 2924 (m), 2857 (w), 1640 (w), 1591 (s), 1578 (s), 1455 (s), 1374 (w), 1219 (w), 1155 (w), 1091 (w), 993 (m), 909 (s), 790 (m), 769 (m), 750 (m) cm^{-1}. ^{1}H NMR (500 MHz, CDCl$_3$): δ = 1.78–1.84 (m, 2 H, 2-H), 2.09–2.15 (m, 2 H, 3-H), 2.53 (s, 3 H, CH$_3$), 2.74–2.78 (m, 2 H, 1-H), 4.96 (ddt, J = 10.3, J = 2.1, J = 1.3 Hz, 1 H, 5-H$_{trans}$), 5.02 (ddt, J = 17.1, J = 2.1, J = 1.5 Hz, 1 H, 5-H$_{cis}$), 5.85 (ddt, J = 17.1, J = 10.3, J = 6.7 Hz, 1 H, 4-H), 6.95 (d, J = 7.8 Hz,

2 H, *m*-H), 7.48 (t, *J* = 7.8 Hz, 2 H, *p*-H) ppm. ^{13}C NMR (125 MHz, CDCl$_3$): δ = 24.6 (CH$_3$), 29.3 (C-2), 33.5 (C-3), 37.9 (C-1), 114.7 (C-5), 119.5 (*m*-CH), 120.4 (*m*-CH), 136.5 (C-4), 138.5 (*p*-CH), 157.8 (*o*-C), 161.6 (*o*-C) ppm. MS (ESI): *m/z* = 176.1, 170.1, 162.1 [M + H]$^+$, 148.1, 120.1, 107.1. HRMS (ESI): calcd. for C$_{11}$H$_{16}$N 162.1277; found 162.1270.

Methyl 4-[6-(4-Methoxy-4-oxobutyl)pyridin-2-yl]butanoate (4b): Ozone was passed through a stirred solution of **7** (500 mg, 2.32 mmol) in CH$_2$Cl$_2$ (20 mL) and NaOH/MeOH (2.5 M, 5 mL) at –78 °C until the mixture became blue. It was then diluted with EtOAc/H$_2$O (1:1) and warmed up to room temperature. The aqueous layer was extracted with EtOAc (3 × 20 mL), and the combined organic layers were dried (MgSO$_4$) and concentrated under reduced pressure. The residue was chromatographed on SiO$_2$ with hexanes/ EtOAc (5:1) to yield **4b** as a colorless liquid (173 mg, 0.62 mmol, 27%). R_f = 0.27. FTIR (ATR): ṽ = 2951 (m), 1731 (vs), 1590 (m), 1576 (m), 1455 (m), 1436 (m), 1368 (m), 1314 (m), 1244 (m), 1197 (s), 1070 (m), 1139 (s), 1055 (m), 991 (m), 864 (m) cm^{-1}. ^{1}H NMR (500 MHz, CDCl$_3$): δ = 2.05 (tt, *J* = 7.6, *J* = 7.6 Hz, 4 H, 2-H), 2.38 (t, *J* = 7.6 Hz, 4 H, 3-H), 2.79 (t, *J* = 7.6 Hz, 4 H, 1-H), 3.67 (s, 6 H, OCH$_3$), 6.97 (d, *J* = 7.7 Hz, 2 H, *m*-H), 7.50 (t, *J* = 7.7 Hz, 2 H, *p*-H) ppm. ^{13}C NMR (125 MHz, CDCl$_3$): δ = 24.9 (C-2), 33.6 (C-3), 37.6 (C-1), 51.7 (OCH$_3$), 120.3 (*m*-CH), 136.8 (*p*-CH), 160.8 (*o*-C), 174.1 (C=O) ppm. MS (ESI): *m/z* = 302.1 [M + Na]$^+$, 280.2 [M + H]$^+$, 248.1, 220.1. HRMS (ESI): calcd. for C$_{15}$H$_{21}$NNaO$_4$ 302.1363; found 302.1355.

General Procedure for the Wittig Reaction: To a solution of the respective phosphonium bromide **3a,b** (2.2 equiv.) and pyridinecarbaldehyde **1** (1 equiv.) in dmf was slowly added dropwise a 2.5 M NaOEt solution (2.4 equiv.), and the reaction mixture stirred at room temperature for 2 h. The reaction mixture was poured into a 1:1 mixture of heptane/H$_2$O. The layers were separated, and the aqueous layer was extracted three times with heptane. The combined organic layers were dried (MgSO$_4$), concentrated under reduced pressure, and chromatographed on SiO$_2$ with hexanes/ EtOAc (5:1).

Ethyl 5-{6-[5-Ethoxy-5-oxopent-1-enyl]pyridin-2-yl}pent-4-enoate (2c): Following the general procedure, **1** (200 mg, 1.48 mmol), bromide **3a** (1.440 g, 3.26 mmol), and NaOEt (1.5 mL, 3.63 mmol) in dmf (6 mL) yielded **2c** as a yellowish liquid (mixture of all-*trans*, all-*cis*, *cis/trans*, 1:3:3) (348 mg, 1.05 mmol, 71%). R_f = 0.2–0.25. FTIR (ATR): ṽ = 2980 (m), 2932 (m), 1777 (m), 1726 (vs), 1655 (m), 1566 (m), 1450 (m), 1371 (m), 1348 (m), 1301 (m), 1251 (m), 1156 (s), 1095 (m), 1027 (m), 971 (s), 855 (m) cm^{-1}. ^{1}H NMR (500 MHz, CDCl$_3$): δ = 1.21–1.28 (m, 6 H, OCH$_2$C*H$_3$*), 2.47–2.61 (m, 5.6 H, 3-H$_{trans}$, 4-H), 2.95–3.04 (m, 2.4 H, 3-H$_{cis}$), 4.10–4.17 (m, 4 H, OC*H$_2$*CH$_3$), 5.83 (dt, *J* = 11.7, *J* = 7.3 Hz, 0.7 H, 2-H$_{cis}$), 5.87 (dt, *J* = 11.7, *J* = 7.3 Hz, 0.7 H, 2-H$_{cis}$), 6.42–6.48 (m, 1.3 H, 1-H$_{cis}$), 6.51 (d, *J* = 15.5 Hz, 0.7 H, 1-H$_{trans}$), 6.75 and 6.76 (dt, *J* = 15.5, *J* = 6.8 Hz, 0.7 H, 2-H$_{trans}$), 7.02–7.07 (m, 2 H, *m*-CH), 7.51–7.60 (m, 1 H, *p*-H) ppm. ^{13}C NMR (125 MHz, CDCl$_3$): δ = 14.2, 14.3 (OCH$_2$CH$_3$), 24.4, 24.6 (C-3$_{cis}$), 28.0 (C-3$_{trans}$), 33.7, 34.1, 34.2 (C-4), 60.3, 60.4, 60.5 (OCH$_2$CH$_3$), 119.0, 119.5, 121.9, 122.3 (*m*-CH), 129.4, 129.7, 131.0 (C-1), 133.2 (C-2$_{trans}$), 134.5, 134.9 (C-2$_{cis}$), 136.2, 136.5 (*p*-CH), 155.0, 155.8, 156.0 (*o*-C), 172.9, 173.2, 173.3 (C=O) ppm. MS (ESI): *m/z* = 354.2 [M + Na]$^+$, 332.2 [M + H]$^+$. HRMS (ESI): calcd. for C$_{19}$H$_{25}$NNaO$_4$ 354.1676; found 354.1672.

Ethyl 5-{6-[6-Ethoxy-6-oxohex-1-enyl]pyridin-2-yl}hex-5-enoate (2d): Following the general procedure, **1** (3.231 g, 23.92 mmol), bromide **3b** (23.117 g, 52.61 mmol), and NaOEt (24 mL, 60 mmol) in dmf (100 mL) yielded **2d** as a yellowish liquid (mixture of all-*trans*, all-*cis*, *cis/trans*, 1:3:3) (3.266 g, 10.73 mmol, 40%). FTIR (ATR): ṽ = 2981 (m), 1727 (vs), 1585 (m), 1456 (m), 1374 (m), 1350 (m), 1301 (m), 1178 (s), 1097 (m), 1030 (m), 907 (s), 829 (m) cm^{-1}. ^{1}H NMR (500 MHz, CDCl$_3$): δ = 1.21–1.27 (m, 6 H, OCH$_2$C*H$_3$*), 1.78–1.89 (m, 4 H, 4-H), 2.29–2.39 (m, 5.7 H, 3-H$_{trans}$, 5-H), 2.64–2.75 (m, 2.3 H, 3-H$_{cis}$), 4.08–5.15 (m, 4 H, OC*H$_2$*CH$_3$), 5.83 (dt, *J* = 11.9, *J* = 7.3 Hz, 0.7 H, 2-H$_{cis}$), 5.85 (dt, *J* = 11.9, *J* = 7.3 Hz, 0.7 H, 2-H$_{cis}$), 6.44–6.51 (m, 2 H, 1-H), 6.72 and 6.74 (dt, *J* = 15.6, *J* = 6.8 Hz, 0.7 H, 2-H$_{trans}$), 7.01–7.08 (m, 2 H, *m*-H), 7.54–7.60 (m, 1 H, *p*-H) ppm. ^{13}C NMR (125 MHz, CDCl$_3$): δ = 14.24, 14.3 (OCH$_2$CH$_3$), 24.18, 24.23, 24.98, 24.99 (C-4), 28.2, 28.3 (C-3$_{cis}$), 32.10, 32.14 (C-3$_{trans}$), 33.8, 33.9, 34.0 (C-5), 60.3, 60.25, 60.29 (OCH$_2$CH$_3$), 118.8, 119.2, 121.6, 122.1 (*m*-CH), 129.2, 129.6, 131.0 (C-1), 134.3 (C-2$_{trans}$), 135.6 (C-2$_{cis}$), 136.0, 136.5 (*p*-CH), 155.1, 155.9, 156.1 (*o*-C), 173.5, 173.6, 173.7 (C=O) ppm. MS (EI): *m/z* (%) = 359.2 (52) [M]$^+$, 330.2 (8), 314.2 (38), 286.2 (12), 272.2 (100), 244.1 (5), 226.1 (9), 204.1 (6), 184.1 (7), 170.1 (11), 154.1 (7), 130.1 (3), 77.0 (2), 55.0 (2). HRMS (ESI): calcd. for C$_{21}$H$_{30}$NO$_4$ 360.2169; found 360.2164.

General Procedure for the Hydrogenation of Alkenoates 2: A suspension of the respective **2** and Pd/C (15 mg, 10%) in absolute MeOH (5 mL) was hydrogenated at room temperature under 1 bar hydrogen. After 15 h, the reaction mixture was filtered through SiO$_2$ with EtOAc as eluent, and the filtrate was concentrated under reduced pressure.

Methyl 3-[6-(3-Methoxy-3-oxopropyl)pyridin-2-yl]propanoate (4a): Following the general procedure, **2a** (400 mg, 1.59 mmol) yielded **4a** as a yellowish liquid (391 mg, 1.56 mmol, 98%). FTIR (ATR): ṽ = 2952 (m), 2846 (w), 1730 (vs), 1592 (m), 1576 (m), 1456 (m), 1436 (s), 1363 (m), 1309 (m), 1194 (s), 1158 (vs), 1094 (m), 1030 (m), 988 (m), 879 (w), 842 (m), 805 (m) cm^{-1}. ^{1}H NMR (500 MHz, CDCl$_3$): δ = 2.79 (t, *J* = 7.5 Hz, 4 H, 2-H) 3.07 (t, *J* = 7.5 Hz, 4 H, 1-H), 3.67 (s, 6 H, OCH$_3$), 6.98 (d, *J* = 7.7 Hz, 2 H, *m*-H), 7.48 (t, *J* = 7.7 Hz, 2 H, *p*-H) ppm. ^{13}C NMR (125 MHz, CDCl$_3$): δ = 32.7 (C-2), 32.9 (C-1), 51.6 (OCH$_3$), 120.4 (*m*-CH), 136.6 (*p*-CH), 159.3 (*o*-C), 173.8 (C=O) ppm. MS (ESI): *m/z* = 274.1 [M + Na]$^+$, 252.1 [M + H]$^+$, 220.1. HRMS (ESI): calcd. for C$_{13}$H$_{17}$NO$_4$ 252.1230; found 252.1221.

Ethyl 3-[6-(5-Ethoxy-5-oxopentyl)pyridin-2-yl]pentanoate (4c): Following the general procedure, **2c** (323 mg, 0.97 mmol) yielded **4c** as a yellowish liquid (316 mg, 0.94 mmol, 97%). R_f = 0.31 (hexanes/ EtOAc, 5:1). FTIR (ATR): ṽ = 2979 (m), 2935 (m), 2863 (w), 1729 (vs), 1590 (m), 1576 (m), 1455 (m), 1372 (m), 1349 (m), 1302 (m), 1177 (s), 1096 (m), 1058 (m), 1029 (m), 917 (w), 857 (w), 785 (m), 753 (m) cm^{-1}. ^{1}H NMR (500 MHz, CDCl$_3$): δ = 1.25 (t, *J* = 7.2 Hz, 6 H, OCH$_2$C*H$_3$*), 1.66–1.78 (m, 8 H, 2-H, 3-H), 2.33 (t, *J* = 7.2 Hz, 4 H, 4-H), 2.77 (t, *J* = 7.4 Hz, 4 H, 1-H), 4.11 (q, *J* = 7.2 Hz, 4 H, OC*H$_2$*CH$_3$), 6.95 (d, *J* = 7.6 Hz, 2 H, *m*-H), 7.48 (t, *J* = 7.6 Hz, 2 H, *p*-H) ppm. ^{13}C NMR (125 MHz, CDCl$_3$): δ = 14.3 (OCH$_2$CH$_3$), 24.7 (C-2 or C-3), 29.5 (C-2 or C-3), 34.2 (C-4), 38.1 (C-1), 60.2 (OCH$_2$CH$_3$), 119.8 (*m*-C), 136.5 (*p*-C), 161.3 (*o*-C), 173.7 (C=O) ppm. MS (ESI): *m/z* = 358.2 [M + Na]$^+$, 336.2 [M + H]$^+$. HRMS (ESI): calcd. for C$_{19}$H$_{30}$NO$_4$ 336.2169; found 336.2166.

Ethyl 3-[6-(6-Ethoxy-6-oxohexyl)pyridin-2-yl]hexanoate (4d): Following the general procedure, **2d** (2.11 g, 5.88 mmol) yielded **4d** as a colorless liquid (2.10 g, 5.79 mmol, 98%). R_f = 0.36 (hexanes/ EtOAc, 5:1). FTIR (ATR): ṽ = 2980 (m), 2933 (m), 2858 (m), 1730 (vs), 1590 (m), 1576 (m), 1455 (m), 1372 (m), 1347 (m), 1299 (m), 1247 (m), 1177 (s), 1097 (m), 1031 (m), 859 (m) cm^{-1}. ^{1}H NMR (500 MHz, CDCl$_3$): δ = 1.24 (t, *J* = 7.1 Hz, 6 H, OCH$_2$C*H$_3$*), 1.38–

1.43 (m, 4 H, 3-H), 1.64–1.75 (m, 8 H, 2-H, 4-H), 2.29 (t, J = 7.5 Hz, 4 H, 5-H), 2.75 (t, J = 7.8 Hz, 4 H, 1-H), 4.11 (q, J = 7.1 Hz, 4 H, OCH_2CH$_3$), 6.94 (d, J = 7.6 Hz, 2 H, m-H), 7.49 (t, J = 7.6 Hz, 2 H, p-H) ppm. ^{13}C NMR (125 MHz, CDCl$_3$): δ = 14.3 (OCH$_2$$CH_3$), 24.9 (C-4), 28.9 (C-3), 29.8 (C-2), 34.3 (C-5) 38.3 (C-1), 60.2 (OCH$_2$CH$_3$), 119.7 (m-CH), 136.5 (p-CH), 161.6 (o-C), 173.8 (C=O) ppm. MS (ESI): m/z = 364.2 [M + H]$^+$, 336.2, 318.2, 308.2, 290.2, 272.2, 262.2, 244.2, 216.2, 120.1. HRMS (ESI): calcd. for C$_{21}$H$_{34}$NO$_4$ 364.2482; found 364.2478.

General Procedure for the Preparation of Hydrochlorides (5·HCl): A solution of the respective **4** in concentrated hydrochloric acid (150 mL) and H$_2$O (100 mL) was heated at reflux for 24 h. All volatile materials were removed under vacuum, and the remaining solid was recrystallized from H$_2$O.

2,6-Pyridinedipropanoic Acid Hydrochloride (5a·HCl): Following the general procedure, **4a** (10.16 g, 40.4 mmol) yielded **5a·HCl** as a colorless solid (8.22 g, 31.7 mmol, 78%). M.p. 193 °C. FTIR (ATR): $\tilde{v}$ = 3034 (m), 2859 (m), 2780 (m), 1887 (w), 1732 (vs), 1642 (s), 1623 (s), 1396 (s), 1263 (m), 1213 (m), 1196 (m), 1150 (s), 1019 (m), 951 (m), 808 (s), 759 (s) cm^{-1}. ^{1}H NMR (500 MHz, D$_2$O): δ = 2.95 (t, J = 7.2 Hz, 4 H, 2-H), 3.33 (t, J = 7.2 Hz, 4 H, 1-H), 7.78 (d, J = 8.0 Hz, 2 H, m-H), 8.39 (t, J = 8.0 Hz, 2 H, p-H) ppm. ^{13}C NMR (125 MHz, D$_2$O): δ = 27.8 (C-1), 32.2 (C-2), 124.6 (m-CH), 146.7 (p-CH), 155.1 (o-C), 175.7 (C=O) ppm. MS (ESI): m/z = 246.1 [C$_{11}$H$_{13}$NNaO$_4$]$^+$, 224.1 [C$_{11}$H$_{14}$NO$_4$]$^+$, 206.1. C$_{11}$H$_{14}$ClNO$_4$ (259.69): calcd. C 50.88, H 5.43, N 5.39; found C 50.63, H 5.44, N 5.35.

2,6-Pyridinedibutanoic Acid Hydrochloride (5b·HCl): Following the general procedure, **4b** (940 mg, 3.37 mmol) yielded **5b·HCl** as a colorless solid (861 mg, 2.99 mmol, 89%). M.p. 183 °C. FTIR (ATR): $\tilde{v}$ = 3026 (s), 2970 (s), 2749 (s), 1895 (w), 1722 (vs), 1637 (s), 1622 (s), 1543 (w), 1455 (w), 1418 (m), 1392 (s), 1368 (m), 1319 (w), 1248 (s), 1215 (m), 1166 (s), 1139 (s), 1055 (m), 956 (w), 813 (s), 782 (s) cm^{-1}. ^{1}H NMR (500 MHz, CDCl$_3$): δ = 1.93 (tt, J = 7.3, J = 7.3 Hz, 4 H, 2-H), 2.34 (t, J = 7.3 Hz, 4 H, 3-H), 2.93 (t, J = 7.3 Hz, 4 H, 1-H), 7.59 (d, J = 7.9 Hz, 2 H, m-H), 8.21 (t, J = 7.9 Hz, 2 H, p-H) ppm. ^{13}C NMR (125 MHz, CDCl$_3$): δ = 23.6 (C-2), 31.9 (C-1), 32.5 (C-3), 124.7 (m-CH), 146.6 (p-CH), 156.0 (o-C), 177.3 (C=O) ppm. MS (ESI): m/z = 274.1 [C$_{13}$H$_{17}$NNaO$_4$]$^+$, 252.1 [C$_{13}$H$_{18}$NO$_4$]$^+$, 234.1, 220.1, 206.1. HRMS (ESI): calcd. for C$_{13}$H$_{18}$NO$_4$ 252.1230; found 252.1242.

2,6-Pyridinedipentanoic Acid Hydrochloride (5c·HCl): Following the general procedure, **4c** (1 g, 2.98 mmol) yielded **5c·HCl** as a yellowish solid (878 mg, 2.78 mmol, 93%). M.p. 174 °C. FTIR (ATR): $\tilde{v}$ = 3061 (m), 2955 (m), 2845 (m), 2735 (m), 1930 (w), 1923 (w), 1770 (w), 1731 (vs), 1637 (s), 1617 (s), 1467 (m), 1420 (m), 1395 (m), 1348 (m), 1292 (m), 1236 (m), 1163 (s), 1139 (s), 1078 (m), 1051 (m), 974 (m), 882 (w), 807 (s), 766 (s) cm^{-1}. ^{1}H NMR (500 MHz, D$_2$O): δ = 1.64–1.70 (m, 4 H, 3-H), 1.80–1.86 (m, 4 H, 2-H), 2.44 (t, J = 7.3 Hz, 4 H, 4-H), 3.07 (t, J = 7.6 Hz, 4 H, 1-H), 7.74 (d, J = 8.0 Hz, 2 H, m-H), 8.37 (t, J = 8.0 Hz, 2 H, p-H) ppm. ^{13}C NMR (125 MHz, D$_2$O): δ = 23.4 (C-3), 27.9 (C-2), 32.3 (C-1), 33.3 (C-4), 124.3 (m-CH), 146.5 (p-CH), 156.5 (o-C), 178.4 (C=O) ppm. MS (ESI): m/z = 280.2 [C$_{15}$H$_{22}$NO$_4$]$^+$. C$_{15}$H$_{22}$ClNO$_4$ (315.79): calcd. C 57.05, H 7.02, Cl 11.23, N 4.44; found C 56.87, H 7.01, Cl 11.34, N 4.32.

2,6-Pyridinedihexanoic Acid Hydrochloride (5d·HCl): Following the general procedure, **4d** (1.12 g, 3.07 mmol) yielded **5d·HCl** as a colorless solid (1.00 mg, 2.92 mmol, 95%). M.p. 142 °C. FTIR (ATR): $\tilde{v}$ = 3058 (m), 2952 (m), 2935 (m), 2862 (m), 2775 (m), 2707 (m), 1949 (w), 1923 (w), 1778 (w), 1726 (vs), 1634 (s), 1620 (s), 1386 (s), 1279 (m), 1237 (m), 1221 (m), 1159 (s), 1127 (s), 1078 (m), 982 (m),

821 (s), 788 (s) cm^{-1}. ^{1}H NMR (500 MHz, D$_2$O): δ = 1.34–1.00 (m, 4 H, 3-H), 1.59–1.65 (m, 4 H, 4-H), 1.76–1.82 (m, 4 H, 2-H), 2.35 (t, J = 7.3 Hz, 4 H, 5-H), 3.02 (t, J = 7.6 Hz, 4 H, 1-H), 7.70 (d, J = 8.0 Hz, 2 H, m-H), 8.33 (t, J = 8.0 Hz, 2 H, p-H) ppm. ^{13}C NMR (125 MHz, CDCl$_3$): δ = 23.9 (C-4), 27.4 (C-3), 28.2 (C-2), 32.5 (C-5) 33.9 (C-1), 124.3 (m-CH), 146.3 (p-CH), 156.9 (o-C), 179.5 (C=O) ppm. MS (ESI): m/z = 330.17 [C$_{17}$H$_{25}$NNaO$_4$]$^+$, 308.19 [C$_{17}$H$_{26}$NO$_4$]$^+$, 290.17. HRMS (ESI): calcd. for C$_{17}$H$_{26}$NO$_4$ 308.1856; found 308.1857. C$_{17}$H$_{26}$ClNO$_4$ (343.85): calcd. C 59.38, H 7.62, Cl 10.31, N 4.07; found C 59.19, H 7.67, Cl 10.39, N 3.97.

General Procedure for the Preparation of Iron Complexes (8): Under N$_2$, a solution of the respective hydrochloride **5** (1 equiv.) and LiOH (2 equiv.) in absolute MeOH (3 mL) was stirred at room temperature for 20 min. The solvent was removed under reduced pressure, and the residue dried under vacuum. The residue was then taken up in absolute MeOH (1.8 mL), and a 2.5 M solution of iron(III)nitrate, which was dried under vacuum, was added dropwise. After stirring for 5 min, the precipitate was filtered off.

[Fe$_3$(μ$_3$-O)(5aH)$_3$Cl$_{1.5}$](NO$_3$)$_{2.5}$·6H$_2$O (8a): Following the procedure described above, **5a** (250 mg, 0.963 mmol) yielded **8a** as a red–orange solid (254 mg, 0.218 mmol, 68%). M.p. 238 °C (dec.). FTIR (ATR): $\tilde{v}$ = 3191 (m), 3086 (m), 2922 (m), 1969 (w), 1730 (w), 1645 (m), 1595 (s), 1540 (w), 1435 (s), 1402 (s), 1295 (s), 1172 (m), 1015 (m), 984 (m), 870 (w), 809 (m), 744 (w), 670 (w), 579 (m) cm^{-1}. UV/Vis (H$_2$O): λ_{max} (logε_{max}) = 269 (4.70). MS (ESI): m/z = 865.02 [C$_{33}$H$_{35}$Fe$_3$N$_3$O$_{14}$]$^+$, 847.01 [C$_{33}$H$_{33}$Fe$_3$N$_3$O$_{13}$]$^+$. HRMS (ESI): calcd. for C$_{33}$H$_{33}$Fe$_3$N$_3$O$_{13}$ 847.0058; found 847.0056. C$_{33}$H$_{36}$Cl$_{1.5}$Fe$_3$N$_{5.5}$O$_{20.5}$·6H$_2$O (1166.47): calcd. C 33.98, H 4.15, Cl 4.56, N 6.60; found C 33.93, H 4.04, Cl 4.64, N 6.64.

[Fe$_3$(μ$_3$-O)(5bH)$_3$Cl](NO$_3$)$_3$·7H$_2$O (8b): Following the procedure described above, **5b** (150 mg, 0.521 mmol) yielded **8b** as a red–orange solid (165 mg, 0.129 mmol, 74%). M.p. 233 °C (dec.). FTIR (ATR): $\tilde{v}$ = 3191 (m), 3086 (m), 2922 (m), 1969 (w), 1730 (w), 1645 (m), 1595 (s), 1540 (w), 1435 (s), 1402 (s), 1295 (s), 1172 (m), 1015 (m), 984 (m), 870 (w), 809 (m), 744 (w), 670 (w), 579 (m) cm^{-1}. UV/Vis (H$_2$O): λ_{max} (logε_{max}) = 270 (4.41). MS (ESI): m/z = 931.10 [C$_{39}$H$_{45}$Fe$_3$N$_3$O$_{13}$]$^+$. HRMS (ESI): calcd. for C$_{39}$H$_{45}$Fe$_3$N$_3$O$_{13}$ 931.0998; found 931.0983. C$_{39}$H$_{48}$ClFe$_3$N$_6$O$_{22}$·7H$_2$O (1281.92): calcd. C 36.54, H 4.87, Cl 2.77, N 6.56; found C 36.66, H 4.95, Cl 3.16, N 6.47.

[Fe$_3$(μ$_3$-O)(5cH)$_3$Cl](NO$_3$)$_3$·6H$_2$O (8c): Following the procedure described above, **5c** (276 mg, 0.921 mmol) yielded **8c** as a red–orange solid (306 mg, 0.227 mmol, 78%). M.p. 229 °C (dec.). FTIR (ATR): $\tilde{v}$ = 3084 (m), 2935 (m), 1967 (w), 1729 (w), 1644 (m), 1587 (s), 1416 (s), 1297 (s), 1173 (m), 1017 (m), 878 (w), 824 (w), 805 (w), 774 (w), 670 (w), 598 (m), 586 (m) cm^{-1}. UV/Vis (H$_2$O): λ_{max} (logε_{max}) = 272 (4.55). MS (ESI): m/z = 1047.22 [C$_{46}$H$_{61}$Fe$_3$N$_3$O$_{14}$]$^+$, 1033.20 [C$_{45}$H$_{59}$Fe$_3$N$_3$O$_{14}$]$^+$, 1015.19 [C$_{45}$H$_{57}$Fe$_3$N$_3$O$_{13}$]$^+$, 499.09, 294.15. HRMS (ESI): calcd. for C$_{45}$H$_{57}$Fe$_3$N$_3$O$_{13}$ 1015.1938; found 1015.1934. C$_{45}$H$_{60}$ClFe$_3$N$_6$O$_{22}$·6H$_2$O (1348.07): calcd. C 40.09, H 5.38, Cl 2.63, N 6.23; found C 40.30, H 5.44, Cl 3.04, N 6.26.

[Fe$_3$(μ$_3$-O)(5dH)$_3$Cl](NO$_3$)$_3$·6H$_2$O (8d): Following the procedure described above, **5d** (228 mg, 0.663 mmol) yielded **8d** as a red–orange solid (286 mg, 0.200 mmol, 90%). M.p. 223 °C (dec.). FTIR (ATR): $\tilde{v}$ = 3098 (m), 2934 (m), 2861 (m), 1975 (w), 1731 (w), 1645 (m), 1622 (m), 1588 (s), 1416 (s), 1302 (s), 1172 (m), 1138 (w), 1019 (m), 824 (w), 736 (w), 713 (w), 671 (w), 590 (m) cm^{-1}. UV/Vis (H$_2$O): λ_{max} (logε_{max}) = 272 (4.72). MS (ESI): m/z = 1099.29 [C$_{51}$H$_{69}$Fe$_3$N$_3$O$_{13}$]$^+$, 336.21, 322.19, 290.16. HRMS (ESI): calcd. for C$_{51}$H$_{69}$Fe$_3$N$_3$O$_{13}$: 1099.2877; found 1099.2857.

$C_{51}H_{72}ClFe_3N_6O_{22}\cdot6H_2O$ (1432.23): calcd. C 42.77, H 5.91, Cl 2.48, N 5.87; found C 42.65, H 5.75, Cl 2.61, N 5.92.

[Fe$_4$(μ_3-O)$_2$(5aH)$_2$Cl$_2$(H$_2$O)$_8$](NO$_3$)$_4$·3H$_2$O (9): A solution of **8a** (50 mg, 0.042 mmol) in H_2O (1 mL) was heated at reflux for 5 min. After concentration of the solvent, **9** precipitated within 4 weeks under an O_2 atmosphere as red crystals (20 mg, 0.016 mmol, 51%). M.p. 253 °C (dec.). FTIR (ATR): $\tilde{v}$ = 3509 (m), 3301 (s), 3202 (s), 3104 (s), 2364 (w), 2182 (w), 1974 (w), 1661 (w), 1642 (m), 1620 (m), 1532 (s), 1434 (s), 1412 (s), 1388 (vs), 1339 (s), 1291 (vs), 1228 (s), 1167 (m), 1055 (w), 1036 (w), 979 (m), 934 (w), 810 (m), 749 (w), 670 (w), 637 (m), 607 (m) 568 (m) cm^{-1}. UV/Vis (H_2O): λ_{max} (logε_{max}) = 271 (4.83). MS (ESI): m/z = 865.01 [$C_{33}H_{35}Fe_3N_3O_{14}$]$^+$, 847.00 [$C_{33}H_{33}Fe_3N_3O_{13}$]. (In solution **9** may exist as **8a**). $C_{22}H_{24}Cl_2Fe_4N_6O_{22}\cdot11H_2O$ (1216.91): calcd. C 21.71, H 3.81, N 6.91; found C 21.65, H 3.64, N 7.03. For structural data see Table 5.

Table 5. Crystallographic data and structure parameters for complexes **9** and **10**.[38]

	9	10
Formula	$C_{22}H_{44}Cl_2Fe_4N_6O_{32}$	$C_{44}H_{52}Cl_3Fe_3N_4O_{33}$[a]
F_w	1198.93	1438.80
Crystal system	triclinic	monoclinic
Space group	$P\bar{1}$	$P2(1)$
a [Å]	8.6620(10)	14.727(3)
b [Å]	10.8833(10)	15.287(3)
c [Å]	12.2691(10)	14.774(3)
α [°]	99.726(7)	90
β [°]	95.249(8)	117.654(14)
γ [°]	107.687(8)	90
V [Å^3]	1073.48(18)	2946.1(10)
Z	1	2
$D_{calcd.}$ [gcm^{-3}]	1.855	1.622
μ [mm^{-1}]	1.561	0.964
$F(000)$	612	1474
Reflections collected	9943	12028
Independent reflections	9438	11573
GOF on F^2	1.071	1.052
$R[I>2\sigma(I)]$	$R_1 = 0.0549$	$R_1 = 0.0666$
	$wR_2 = 0.1017$	$wR_2 = 0.1402$
R(all data)	$R_1 = 0.0825$	$R_1 = 0.0941$
	$wR_2 = 0.1104$	$wR_2 = 0.1541$

[a] Solvent water molecules are strongly disordered. Thus, a different result with other analytical methods could be possible due to polymorphic effects.

[Fe$_3$(μ_3-O)(5a)$_4$(H$_2$O)](ClO$_4$)$_3$·4H$_2$O (10): A solution of **5a**·HCl (215 mg, 0.83 mmol) and LiOH (40 mg, 1.67 mmol) in absolute MeOH (2 mL) was stirred at room temperature for 20 min. A solution of Fe(ClO$_4$)$_3$·9H$_2$O (293 mg, 0.83 mmol) in absolute MeOH (0.5 mL) was then added dropwise, and after stirring the mixture for a further 5 min at room temperature, the precipitate was filtered off. The red solid was dissolved in H_2O (3 mL) and heated at reflux for 1 min. After concentration of the solvent, **10** precipitated within 2 weeks under an O_2 atmosphere as red crystals (232 mg, 0.158 mmol, 76%). M.p. 240 °C (dec.). FTIR (ATR): $\tilde{v}$ = 3566 (w), 3424 (w), 3292 (w), 3206 (w), 3089 (w), 2930 (w), 2585 (w), 1974 (w), 1601 (s), 1575 (s), 1537 (s), 1435 (vs), 1396 (vs), 1313 (s), 1217 (w), 1176 (w), 1069 (vs), 976 (s), 946 (m), 875 (m), 811 (m), 799 (m), 754 (m), 711 (m), 620 (s), 580 (s), 562 (m) cm^{-1}. UV/Vis (H_2O): λ_{max} (logε_{max}) = 271 (4.60). MS (ESI): m/z = 1079.09 [$C_{44}H_{46}Cl_3Fe_3N_4O_{17}$]$^+$, 865.02, 847.00, 535.56 [$C_{44}H_{47}Cl_3Fe_3N_4O_{17}$]$^{2+}$, 485.12, 415.01, 379.01. HRMS (ESI):

calcd. for $C_{44}H_{46}Cl_3Fe_3N_4O_{17}$ 1070.0904; found 1070.0905. $C_{44}H_{48}Cl_3Fe_3N_4O_{29}\cdot5H_2O$ (1460.84): calcd. C 36.18, H 4.00, N 3.84; found C 36.26, H 4.09, N 3.83. For structural data see Table 5.

General Procedure for the Oxidation of Substrates 11, 19, and 23:[2b] To a solution of adamantane **11**, α-pinene **23** (2.00 mmol), or cyclohexene **19** (4.83 mmol) and the respective iron catalyst (7 μmol) in pyridine/acetic acid (27 mL/2.3 mL) under anaerobic conditions was added zinc powder (1.31 g, 20.03 mmol), and the reaction mixture was then vigorously stirred under oxygen (1 bar) for 18 h. An aliquot of 5 mL was removed, H_2O (5 mL) was added, and the mixture was extracted with Et$_2$O (3 × 10 mL). The combined organic extracts were washed successively with H_2O (30 mL), 1 M HCl (30 mL), and brine, dried (MgSO$_4$), and filtered off. To the filtrate was added 1 mL of a standardized solution of naphthalene (4.4 mM) in Et$_2$O (for **11**) or hexadecane (6.2 mM) in Et$_2$O (for **19**), and the mixture was analyzed by gas chromatography. In the case of pinene **23**, the filtrate was directly analyzed by GC, and the product ratio determined by addition of a defined amount of **24**. The retention times were compared to authentic samples of the products.

EXAFS Studies: The EXAFS and XANES measurements were performed at the XAS beamline at the Ångströmquelle Karlsruhe (ANKA) under ambient conditions at 20 °C. The synchrotron beam current was between 80–140 mA at 2.5 GeV storage ring energy. A Si(111) double crystal monochromator was used for measurements at the Fe-K edge (7.112 keV). The second monochromator crystal was tilted for optimal harmonic rejection. The energy resolution for the Fe-K edge energy is estimated to be 1.0 eV. The spectra were recorded in transmission mode with ionisation chambers. All three chambers were filled with nitrogen gas. The individual pressures were adjusted to optimize the signal-to-noise ratio. Energy calibration was performed with an iron metal foil. To avoid mistakes in the XANES region arising from small changes in the energy calibration between two measurements, all spectra were corrected to the theoretical edge energy of iron foil, which was measured in every scan. The solid samples were embedded in a cellulose matrix and pressed into pellets.

Data evaluation started with background absorption removal from the experimental absorption spectrum by subtracting a victoreen-type polynomial. The background-subtracted spectrum was then convoluted with a series of increasingly broader Gauss functions, and the common intersection point was taken as the threshold energy.[39] To determine the smooth part of the spectrum, corrected for pre-edge absorption, a piecewise polynomial was used. It was adjusted in such a way that the low-R components of the resulting Fourier transform were minimal. After division of the background-subtracted spectrum by its smooth part, the photon energy was converted to photoelectron wave numbers k. The resulting $\chi(k)$ function was weighted with k^3. Data analysis was performed in k space on Fourier-filtered data according to the curved wave formalism of the EXCURV98 program with the XALPHA phase and amplitude functions.[40] The window used in the Fourier filter process is given in Table 1. Each shell of individual backscatterers was filtered out and analyzed separately in order to avoid interference from other shells and noise. The mean free path of the scattered electrons was calculated from the imaginary part of the potential (VPI set to –4.00). The amplitude reduction factor S_0^2[41] of the adjusted shells was determined by setting the coordination numbers of the sample **9a** to the expected values of the proposed structure, shown in Scheme 2, and by iterating the distances, Debye–Waller factor, and S_0^2. For the oxygen and carbon shell, a value of 0.8 was

determined, while the carbon and the iron shell require an amplitude reduction factor of 0.62 and 0.42, respectively.

Mössbauer Spectra: The measurements were performed in a He bath cryostat with source and absorber in liquid He at 4.2 K. The source was a standard 50 mCi ^{57}Co/Rh source as delivered by Ritverc (Russia). Spectra were taken of the solid nitrate complex **9a** as well as of frozen solutions after addition of different components (pyridine, cyclohexene **20** under N_2 gas, acetic acid, Zn, O_2 gas) and at different reaction times for the oxidation of cyclohexene.[36a] The solutions were freeze-quenched by dropping the Teflon holders into liquid nitrogen.

^{57}Fe Mössbauer spectra on **10** were recorded on an alternating constant-acceleration spectrometer. The minimal line-width was 0.24 mm s^{-1} full-width at half-height. The sample temperature was maintained constant in a bath cryostat (Wissel MBBC-HE0106). ^{57}Co/Rh was used as the radiation source. Isomer shifts were determined relative to α-iron at room temperature.

Magnetic Studies: Temperature-dependent magnetic susceptibilities of powdered **10** were measured by using a SQUID magnetometer (Quantum Design MPMS-7XL EC) at 1.0 T (2.0–300 K). For calculations of the molar magnetic susceptibility, χ_M, the measured susceptibilities were corrected for the underlying diamagnetism of the sample by using tabulated Pascal's constants. The magnetization data were analyzed on the basis of the usual spin-Hamiltonian description for the electronic ground state by using the simulation package julX written by Eckhard Bill (Max Planck Institute for Bioinorganic Chemistry) for exchange-coupled systems.[42] Magnetic moments were obtained from numerically generated derivatives of the eigenvalues of the spin-Hamiltonian, and summed up over 16 field orientations along a 16-point Lebedev grid to account for the powder distribution of the sample. Intermolecular interactions were considered by using a Weiss temperature, θ_W, as perturbation of the temperature scale, $kT' = k(T - \theta_W)$.

EPR Studies: EPR spectra were recorded on a Bruker EMX X-band spectrometer with an ESR900 continuous flow cryostat from Oxford Instruments. To avoid saturation of the signals, an optimised power of 1 mW was chosen for the experiments. The modulation amplitude was set to 4 G. The sample was diluted in dimethyl formamide until no line broadening resulting from spin exchange was observed anymore. For the measurements, the concentration of the complex was 7.0×10^{-3} mol L^{-1} (10 mg mL^{-1}). The oxygen was removed by four freeze-pump-thaw cycles in the EPR tube.

Supporting Information (see footnote on the first page of this article): Crystal data and structure parameter of ligands **5a–d**, Fourier-filtered $k^3 \cdot \chi(k)$ signals of Fe–O, Fe–C and Fe–Fe shells and back-transformed pseudoradial distribution functions of **8a–d**, Mössbauer spectrum of **8a** at room temperature, freeze-quench Mössbauer data from ref.[36a] and NIS data, and oxidation of adamantane under Gif-type conditions are presented.

Acknowledgments

[1] Reviews: a) L. Que, W. B. Tolman, *Nature* **2008**, *455*, 333–340; b) A. Roth, W. Plass, *Angew. Chem. Int. Ed.* **2008**, *47*, 7588–7591; *Angew. Chem.* **2008**, *120*, 7700–7703; c) R. N. Austin, K. Luddy, K. Erickson, M. Pender-Cudlip, E. Bertrand, D. Deng, R. S. Buzdygon, J. B. van Beilen, J. T. Groves, *Angew. Chem. Int. Ed.* **2008**, *47*, 5232–5234; *Angew. Chem.* **2008**, *120*, 5310–5312; d) J. P. Emerson, E. R. Farquhar, L. Que, *Angew. Chem. Int. Ed.* **2007**, *46*, 8553–8556; *Angew. Chem.* **2007**, *119*, 8705–8708; e) W. Nam, *Acc. Chem. Res.* **2007**, *40*, 522–531; f) J. T. Groves, *J. Inorg. Biochem.* **2006**, *100*, 434–447; g) R. N. Austin, D. Deng, Y. Jiang, K. Luddy, J. B. van Beilen, P. R. Ortiz de Montellano, J. T. Groves, *Angew. Chem. Int. Ed.* **2006**, *45*, 8192–8194; *Angew. Chem.* **2006**, *118*, 8372–8374; h) E. Bertrand, R. Sakai, E. Rozhkova-Novosad, L. Moe, B. G. Fox, J. T. Groves, R. N. Austin, *J. Inorg. Biochem.* **2005**, *99*, 1998–2006; i) E. Y. Tshuva, S. J. Lippard, *Chem. Rev.* **2004**, *104*, 987–1012; j) M. Costas, M. P. Mehn, M. P. Jensen, L. Que, *Chem. Rev.* **2004**, *104*, 939–986; k) C. Limberg, *Angew. Chem. Int. Ed.* **2003**, *42*, 5932–5954; *Angew. Chem.* **2003**, *115*, 6112–6136; l) E. I. Solomon, T. C. Brunold, M. I. Davis, J. N. Kemsley, S.-K. Lee, N. Lehnert, F. Neese, A. J. Skulan, Y.-S. Yang, J. Zhou, *Chem. Rev.* **2000**, *100*, 235–349.

[2] a) D. H. R. Barton, *Tetrahedron* **1998**, *54*, 5805–5817; b) D. H. R. Barton, J. Boivin, M. Gastiger, J. Morzycki, R. S. Hay-Motherwell, W. B. Motherwell, N. Ozbalik, K. M. Schwartzentruber, *J. Chem. Soc. Perkin Trans. 1* **1986**, 947–955; c) D. H. R. Barton, M. J. Gastiger, W. B. Motherwell, *J. Chem. Soc., Chem. Commun.* **1983**, 41–43; d) D. H. R. Barton, R. S. Hay-Motherwell, W. B. Motherwell, *Tetrahedron Lett.* **1983**, *24*, 1979–1982.

[3] C. T. Dziobkowski, J. T. Wrobleski, D. B. Brown, *Inorg. Chem.* **1981**, *20*, 679–684.

[4] Selected reviews on mono- and dinuclear iron complexes: a) D.-L. Popescu, A. Chanda, M. Stadler, F. Tiago de Oliveira, A. D. Ryabov, E. Münck, E. L. Bominaar, T. J. Collins, *Coord. Chem. Rev.* **2008**, *252*, 2050–2071; b) A. Zecchina, M. Rivallan, G. Berlier, C. Lamberti, G. Ricchiardi, *Phys. Chem. Chem. Phys.* **2007**, *9*, 3483–3499; c) A. Decker, M. D. Clay, E. I. Solomon, *J. Inorg. Biochem.* **2006**, *100*, 697–706; d) S. V. Kryatov, E. V. Rybak-Akimova, S. Schindler, *Chem. Rev.* **2005**, *105*, 2175–2226; e) C. He, Y. Mishina, *Curr. Opin. Chem. Biol.* **2004**, *8*, 201–208; f) J.-U. Rohde, M. R. Bukowski, L. Que, *Curr. Opin. Chem. Biol.* **2003**, *7*, 674–682; g) R. Yamahara, S. Ogo, H. Masuda, Y. Watanabe, *J. Inorg. Biochem.* **2002**, *88*, 284–294; h) A. E. Martell, J. Perutka, D. Kong, *Coord. Chem. Rev.* **2001**, *216–217*, 55–63; i) A. Marvilliers, S. Poussereau, *J. Nature* **2000**, *12*, 3–7.

[5] a) J. Yoon, S. A. Wilson, Y. K. Jang, M. S. Seo, K. Nehru, B. Hedman, K. O. Hodgson, E. Bill, E. I. Solomon, W. Nam, *Angew. Chem. Int. Ed.* **2009**, *48*, 1257–1260; *Angew. Chem.* **2009**, *121*, 1283–1286; b) L. Bernasconi, E. J. Baerends, *Inorg. Chem.* **2009**, *48*, 527–540; c) I. Siewert, C. Limberg, S. Demeshko, E. Hoppe, *Chem. Eur. J.* **2008**, *14*, 9377–9388; d) S. Tanase, P. Marques-Gallego, W. R. Browne, R. Hage, E. Bouwman, B. L. Feringa, J. Reedijk, *Dalton Trans.* **2008**, 2026–2033; e) T. Inomata, K. Shinozaki, Y. Hayashi, H. Arii, Y. Funahashi, T. Ozawa, H. Masuda, *Chem. Commun.* **2008**, 392–394; f) S. H. Lee, J. H. Han, H. Kwak, S. J. Lee, E. Y. Lee, H. J. Kim, J. H. Lee, C. Bae, S. N. Lee, Y. Kim, C. Kim, *Chem. Eur. J.* **2007**, *13*, 9393–9398; g) D. Piñero, P. Baran, R. Boca, R. Herchel, M. Klein, R. G. Raptis, F. Renz, Y. Sanakis, *Inorg. Chem.* **2007**, *46*, 10981–10989; h) G. Anilkumar, B. Bitterlich, F. G. Gelalcha, M. K. Tse, M. Beller, *Chem. Commun.* **2007**, 289–291; i) F. G. Gelalcha, B. Bitterlich, A. Anilkumar, M. K. Tse, M. Beller, *Angew. Chem. Int. Ed.* **2007**, *46*, 7293–7296; *Angew. Chem.* **2007**, *119*, 7431–7435; j) J. Bautz, P. Comba, C. Lopez de Laorden, M. Menzel, G. Rajaraman, *Angew. Chem. Int. Ed.* **2007**, *46*, 8067–8070; *Angew. Chem.* **2007**, *119*, 8213–8216, and references cited therein; k) V. B. Romakh, B. Therrien, G.

Süss-Fink, G. B. Shul′pin, *Inorg. Chem.* **2007**, *46*, 3166–3175; l) S. Gosiewska, M. Lutz, A. L. Spek, R. J. M. Klein Gebbink, *Inorg. Chim. Acta* **2007**, *360*, 405–417; m) P. Chaudhuri, E. Rentschler, F. Birkelbach, C. Krebs, E. Bill, T. Weyhermüller, U. Flörke, *Eur. J. Inorg. Chem.* **2003**, 541–555; n) A. K. Boudalis, N. Lalioti, G. A. Spyroulias, C. P. Raptopoulou, A. Terzis, A. Bousseksou, V. Tangoulis, J.-P. Tuchagues, S. P. Perlepes, *Inorg. Chem.* **2002**, *41*, 6474–6487; o) P. Stavropoulos, R. Celenligil-Cetin, A. E. Tapper, *Acc. Chem. Res.* **2001**, *34*, 745–752; p) S. B. Marr, R. O. Carvel, D. T. Richens, H.-J. Lee, M. Lane, P. Stavropoulos, *Inorg. Chem.* **2000**, *39*, 4630–4638; q) R. Celenligil-Cetin, R. J. Staples, P. Stavropoulos, *Inorg. Chem.* **2000**, *39*, 5838–5846; r) S. Ito, K. Inoue, M. Mastumoto, *J. Am. Chem. Soc.* **1982**, *104*, 6450–6452; s) R. Wu, M. Poyraz, F. E. Sowrey, C. E. Anson, S. Wocadlo, A. K. Powell, U. A. Jayasooriya, R. D. Cannon, T. Nakamoto, T. Katada, H. Sano, *Inorg. Chem.* **1998**, *37*, 1913–1921; t) A. M. Bond, R. J. H. Clark, D. G. Humphrey, P. Panayiotopoulos, B. W. Skelton, A. H. White, *J. Chem. Soc., Dalton Trans.* **1998**, 1845–1852; u) R. A. Reynolds, W. R. Dunham, D. Coucouvanis, *Inorg. Chem.* **1998**, *37*, 1232–1241; v) B. Singh, J. R. Long, F. Fabrizi de Biani, D. Gatteschi, P. Stavropoulos, *J. Am. Chem. Soc.* **1997**, *119*, 7030–7047; w) B. Singh, J. R. Long, G. C. Papaefthymiou, P. Stavropoulos, *J. Am. Chem. Soc.* **1996**, *118*, 5824–5825; x) D. H. R. Barton, S. D. Bévière, W. Chavasiri, E. Csuhai, D. Doller, W.-G. Liu, *J. Am. Chem. Soc.* **1992**, *114*, 2147–2156; y) G. Balavoine, D. H. R. Barton, J. Boivin, A. Gref, *Tetrahedron Lett.* **1990**, *31*, 659–662.

[6] Non-heme iron complexes in aerobic oxidation a) S. O. Kim, C. V. Sastri, M. S. Seo, J. Kim, W. Nam, *J. Am. Chem. Soc.* **2005**, *127*, 4178–4179; b) A. Ghosh, F. Tiago de Oliveira, T. Yano, T. Nishioka, E. S. Beach, I. Kinoshita, E. Münck, A. D. Ryabov, C. P. Horwitz, T. J. Collins, *J. Am. Chem. Soc.* **2005**, *127*, 2505–2513; c) E. Pardo, F. Lloret, R. Carrasco, M. C. Muñoz, T. Temporal-Sánchez, R. Ruiz-García, *Inorg. Chim. Acta* **2004**, *357*, 2713–2720; d) E. C. Carson, S. J. Lippard, *J. Am. Chem. Soc.* **2004**, *126*, 3412–3413; e) M. A. Walters, V. Vapnyar, A. Bolour, C. Incarvito, A. L. Rheingold, *Polyhedron* **2003**, *22*, 941–946; f) J. Perutka, A. E. Martell, *Anal. Chim. Acta* **2001**, *435*, 385–391; g) Z. Wang, A. E. Martell, R. J. Motekaitis, J. H. Reibenspies, *Inorg. Chim. Acta* **2000**, *300–302*, 378–383.

[7] D. Chen, A. E. Martell, D. McManus, *Can. J. Chem.* **1995**, *73*, 264–274.

[8] a) A. Horn, A. Neves, A. J. Bortoluzzi, V. Drago, W. A. Ortiz, *Inorg. Chem. Commun.* **2001**, *4*, 173–176; b) L. C. Dorsett, C. J. Hawkins, J. A. Grice, M. F. Lavin, P. M. Merefield, D. L. Parry, I. L. Ross, *Biochemistry* **1987**, *26*, 8078–8082; c) S. W. Taylor, J. D. Cashion, L. J. Brown, C. J. Hawkins, G. R. Hanson, *Inorg. Chem.* **1995**, *34*, 1487–1494.

[9] U. Lüning, R. Baumstark, K. Peters, H. G. von Schnering, *Liebigs Ann. Chem.* **1990**, 129–143.

[10] B. Basu, T. Frejd, *Acta Chem. Scand.* **1996**, *50*, 316–322.

[11] F.-T. Chiu, J. W. Ullrich, P. S. Mariano, *J. Org. Chem.* **1984**, *49*, 228–236.

[12] a) R. L. Danheiser, A. L. Helgason, *J. Am. Chem. Soc.* **1994**, *116*, 9471–9479; b) D. A. Bianchi, F. Rúa, T. S. Kaufman, *Tetrahedron Lett.* **2004**, *45*, 411–415.

[13] L. E. Overman, P. J. Jessup, *J. Am. Chem. Soc.* **1978**, *100*, 5179–5185.

[14] T. H. Jones, J. A. Torres, T. F. Spande, H. M. Garraffo, M. S. Blum, R. R. Snelling, *J. Chem. Ecol.* **1996**, *22*, 1221–1236.

[15] a) J. A. Marshall, A. W. Garofalo, *J. Org. Chem.* **1993**, *58*, 3675–3680; b) J. A. Marshall, A. W. Garofalo, R. C. Sedrani, *Synlett* **1992**, 643–645.

[16] a) E. A. Gutkina, V. M. Trukhan, C. G. Pierpont, S. Mkoyan, V. V. Strelets, E. Nordlander, A. A. Shteinman, *Dalton Trans.* **2006**, 492–501; b) V. M. Trukhan, C. G. Pierpont, K. B. Jensen, E. Nordlander, A. A. Shteinman, *Chem. Commun.* **1999**, 1193–1194.

[17] T. E. Westre, P. Kennepohl, J. G. DeWitt, B. Hedman, K. O. Hodgson, E. I. Solomon, *J. Am. Chem. Soc.* **1997**, *119*, 6297–6314.

[18] a) A. L. Roe, D. J. Schneider, R. J. Mayer, J. W. Pyrz, J. Widom, L. Que, *J. Am. Chem. Soc.* **1984**, *106*, 1676–1681; b) C. R. Randall, L. Shu, Y. Chiou, K. S. Hagen, M. Ito, N. Kitajima, R. J. Lachicotte, Y. Zang, L. Que, *Inorg. Chem.* **1995**, *34*, 1036–1039.

[19] a) R. A. Blair, W. A. Goddard, *Phys. Rev. B* **1980**, *22*, 2767–2776; b) C. Brouder, *J. Phys. Condens. Matter* **1990**, *2*, 701–738.

[20] a) J. E. Hahn, R. A. Scott, K. O. Hodgson, S. Doniach, S. R. Desjardins, E. I. Solomon, *Chem. Phys. Lett.* **1982**, *88*, 595–598; b) J. Wong, F. M. Lytle, R. P. Messmer, D. H. Maylotte, *Phys. Rev. B* **1984**, *30*, 5596–5610; c) L.-S. Kau, D.-J. Spira-Solomon, J. E. Penner-Hahn, K. O. Hodgson, E. I. Solomon, *J. Am. Chem. Soc.* **1987**, *109*, 6433–6442.

[21] M. Bauer, T. Kauf, J. Christoffers, H. Bertagnolli, *Phys. Chem. Chem. Phys.* **2005**, *7*, 2664–2670.

[22] M. Benfatto, J. A. Solera, J. Garcia Ruiz, J. Chaboy, *Chem. Phys.* **2002**, *282*, 441–450.

[23] M. Bauer, S. Müller, G. Kickelbick, H. Bertagnolli, *New J. Chem.* **2007**, *31*, 1950–1959.

[24] An offset of +0.235 mm s^{-1} and +0.102 mm s^{-1} for the measurement at 4.4 K and at room temperature, respectively, was added so as to obtain the isomer shift value with respect to α-Fe at room temperature and to facilitate comparison with the literature.

[25] A. K. Boudalis, Y. Sanakis, C. P. Raptopoulou, A. Terzis, J.-P. Tuchagues, S. P. Perlepes, *Polyhedron* **2005**, *24*, 1540–1548.

[26] C.-C. Wu, H.-G. Jang, A. L. Rheingold, P. Gütlich, D. N. Hendrickson, *Inorg. Chem.* **1996**, *35*, 4137–4147.

[27] A. K. Boudalis, Y. Sanakis, F. Dahan, M. Hendrich, J. P. Tuchagues, *Inorg. Chem.* **2006**, *45*, 443–453.

[28] N. N. Greenwood, T. C. Gibbs, *Mössbauer Spectroscopy*, Chapman and Hall, New York, **1971**, pp. 9–11, pp. 50–53.

[29] P. Gütlich, J. Ensling, *Mossbauer spectroscopy. Inorganic Electronic Structure and Spectroscopy, Vol. I* (Eds.: E. I. Solomon, A. B. P. Lever), John Wiley & Sons, New York, **1999**, pp. 161–211.

[30] a) C. J. O′Connor, *Prog. Inorg. Chem.* **1982**, *29*, 203–283; b) A. P. Ginsberg, *Inorg. Chim. Acta Rev.* **1972**, *5*, 45–68; c) J. S. Grifith, *Struct. Bonding (Berlin)* **1972**, *10*, 87–126; d) E. Sinn, *Coord. Chem. Rev.* **1970**, *5*, 313–347.

[31] R. D. Cannon, R. P. White, *Prog. Inorg. Chem.* **1988**, *36*, 195–298.

[32] J. A. Weil, J. R. Bolton, *Electron Paramagnetic Resonance*, Wiley-Interscience, Hoboken, USA, **2007**.

[33] a) D. H. R. Barton, F. Halley, N. Ozbalik, M. Schmitt, E. Young, G. Balavoine, *J. Am. Chem. Soc.* **1989**, *111*, 7144–7149; b) D. H. R. Barton, *Chem. Soc. Rev.* **1996**, *25*, 237–239; c) M. J. Perkins, *Chem. Soc. Rev.* **1996**, *25*, 229–236.

[34] Calculation of turnover numbers (TON): total amount of products [mol] per catalyst [mol].

[35] Inomata and Masuda reported on a dinucleating pivalamide-substituted pyridine ligand, in which the pyridine nitrogen atoms act as equatorial ligands in this non-heme Fe$_2$ complex. For details see ref.[5e]

[36] a) S. Rajagopalan, T. Asthalter, V. Rabe, U. van Bürck, F. E. Wagner, S. Laschat, *Hyperfine Interact.* **2008**, *187*, 35–41; b) S. Rajagopalan, Dissertation, University of Stuttgart, **2009**; c) T. Asthalter, *personal communication*.

[37] M. Högbom, P. Nordlund, *FEBS Lett.* **2004**, *567*, 179–182.

[38] CCDC-734986 and CCDC-734988 contain the supplementary crystallographic data for this paper. These data can be obtained free of charge from The Cambridge Crystallographic Data Centre via www.ccdc.cam.ac.uk/data_request/cif.

[39] a) T. S. Ertel, H. Bertagnolli, S. Hückmann, U. Kolb, D. Peter, *Appl. Spectrosc.* **1992**, *46*, 690–698; b) M. Newville, P. Livins, Y. Yacoby, J. J. Rehr, E. A. Stern, *Phys. Rev. B* **1993**, *47*, 14126–14131.

S. Laschat et al.

[40] N. Binsted, S. S. Hasnain, *J. Synchrotron Radiat.* **1996**, *3*, 185–196.

[41] a) J. J. Rehr, R. C. Albers, *Rev. Mod. Phys.* **2000**, *72*, 621–654; b) M. Roy, S. J. Gurman, *J. Synchrotron Radiat.* **1999**, *6*, 228–230.

[42] The program package julX was used for the spin-Hamiltonian simulations and for fitting the susceptibility data by a full-matrix diagonalization approach; E. Bill, unpublished results.